1948–98 U.S. Hydrological Reanalysis by the Noah Land Data Assimilation System

Y. FAN

RS Information Systems Inc., McLean, Virginia, and Climate Prediction Center/NCEP/NOAA/NWS, Camp Springs, Maryland

H. M. VAN DEN DOOL

Climate Prediction Center/NCEP/NOAA/NWS, Camp Springs, Maryland

D. LOHMANN AND K. MITCHELL

Environmental Modeling Center/NCEP/NOAA/NWS, Camp Springs, Maryland

(Manuscript received 16 August 2004, in final form 6 April 2005)

ABSTRACT

Land surface variables, such as soil moisture, are among the most important components of memory for the climate system. A more accurate and long time series of land surface data is very important for real-time drought monitoring, for understanding land surface–atmosphere interaction, and for improving weather and climate prediction. Thus, the ultimate goal of the present work is to produce a long-term "land reanalysis" with 1) retrospective and 2) real-time update components that are both generated in a manner that remains temporally homogeneous throughout the record. As the first step of the above goal, the retrospective component is reported here. Specifically, a 51-yr (1948–98) set of hourly land surface meteorological forcing is produced and used to execute the Noah land surface model, all on the 1/8° grid of the North American Land Data Assimilation System (NLDAS). The surface forcing includes air temperature, air humidity, surface pressure, wind speed, and surface downward shortwave and longwave radiation, all derived from the National Centers for Environmental Prediction–National Center For Atmospheric Research (NCEP–NCAR) Global Reanalysis. Additionally, a newly improved precipitation analysis is used to provide realistic hourly precipitation forcing on the NLDAS grid. Some unique procedures are described and applied to yield retroactive forcing that is temporally homogeneous over the 51 yr at the spatial and temporal resolution, including a terrain height adjustment that accounts for the terrain differences between the global reanalysis and the NLDAS. The land model parameters and fixed fields are derived from existing high-resolution datasets of vegetation, soil, and orography. The land reanalysis output from the Noah land surface model consists of eight energy balance components and skin temperature, which are output at 3-hourly intervals, and 15 other variables (i.e., water balance components, surface state variables, etc.), which are output at daily intervals for the period of 1 January 1948 through 31 December 1998.

Using soil moisture observations throughout Illinois over 1984–98 as validation, an improvement in the simulated soil moisture (of the Noah model versus a forerunner leaky bucket model) is illustrated in terms of an improved annual cycle (much better phasing) and somewhat higher anomaly correlation for the anomalies, especially in central and southern Illinois. Nonetheless, considerable room for model improvement remains. For example, the simulated anomalies are overly uniform in the vertical compared to the observations, and some likely routes for model improvement in this aspect are proposed.

1. Introduction

The lower boundary conditions of the atmosphere, such as sea surface temperature (SST), soil moisture, soil temperature, and snowpack often have a longer memory than weather itself. For example, an episodic heavy precipitation or snow event can cause an anomaly in soil moisture and its associated land surface and subsurface variables. However, it may take days or even months to dissipate the anomaly through evaporation and other land surface processes. It is well known that soil moisture and snowpack can influence the partitioning of available energy at the land surface, through sensible and latent heat exchanges with the overlying atmosphere, as well as by changing land sur-

Corresponding author address: Yun Fan, Climate Prediction Center, 5200 Auth Road, Rm. 806, Camps Springs, MD 20746.
E-mail: yun.fan@noaa.gov

face albedo, etc. Among the many aspects of land surface conditions, soil moisture has long been suspected to be an important influence on weather and climate predictions, especially during the warm season when land–atmosphere interaction is strong (Reed 1925; Namias 1952; etc.).

The empirical evidence of the importance of land surface boundary conditions inspired researchers to couple the land surface to the atmosphere in atmospheric models (Manabe 1969; Mahrt and Pan 1984; Delworth and Manabe 1988, 1993; Ek et al. 2003). Model sensitivity studies have shown that land surface processes play a potentially important role in weather and climate prediction from lead times of days to months or longer. In recent years, interest in the role of land surface processes in climate on subseasonal-to-interannual time scales has greatly increased (Mintz and Walker 1993; Yeh 1989; Huang and Van den Dool 1993; Huang et al. 1996, hereafter H96; Fennessy and Shukla 1999; Dirmeyer 2000; Koster and Suarez 2001; Koster et al. 2000, 2003). Many investigations suggest that predictions on those time scales cannot depend on atmospheric initial conditions alone, because of its short memory. In addition to sea surface temperature, added predictability would be derived from the slow variations of the land variables, such as soil moisture, especially for areas in the middle-latitude continents during the warm season.

In spite of advances in our knowledge of land–atmosphere interaction, many important scientific issues or questions remain, such as the quantitative understanding of the land surface water and energy budgets on the continental scale (Roads et al. 2003), mainly because of a lack of sufficient observations. Also, quantifying the nonlocal impacts of soil moisture remains a difficult issue. To improve our understanding of land surface processes, we need more accurate land conditions over multidecadal periods.

So far, there is no global in situ observational network for soil moisture and its associated land surface variables. As for the United States, the data density and quality from the national Soil Climate Analysis Network (SCAN) (Schaefer and Paetzold 2001) vary with locations. Moreover, many stations in the SCAN network do not have a long continuous history. Although there are some very limited networks that possess continuous observations from one to two decades (Robock et al. 2000), the land surface variables, such as soil moisture, are not routinely observed. Present techniques for the satellite-based remote sensing of soil moisture are only effective over sparsely vegetated areas and can only measure the water content of the upper few centimeters of soil. The evolution of the soil moisture in this thin layer represents the fast variations of the soil moisture and thus provides little useful memory for medium- to long-term prediction. The Gravity Recovery and Climate Experiment (GRACE) satellite, launched in March 2002, maps the earth's gravity field with much higher accuracy every month, and it also senses deep soil moisture. The initial results are very encouraging (Wahr et al. 2004). However, the dataset from this product is too short at the present time.

The first National Centers for Environmental Prediction–National Center for Atmospheric Research (NCEP–NCAR) Global Reanalysis (hereafter NNGR; Kalnay et al. 1996; Kistler et al. 2001) comes with precipitation and soil moisture. Previous research (such as Fig. 7 of Kanamitsu et al. 2002, as well as the information found online at http://www.cpc.ncep.noaa.gov/soilmst/sm_ill.html) shows that the soil moisture of NNGR is not very good, compared with the observations in Illinois. The main reason is bias in precipitation and surface radiation fields. In the absence of negative feedbacks, the bias can drive soil moisture far away from realistic values. NNGR also uses soil moisture "nudging" to constrain the error in the soil moisture, which can result in nonclosure of the surface water budget (Maurer et al. 2001). Because of widespread bias in precipitation and the nudging problem, neither precipitation nor soil moisture produced by NNGR is of much use. This is the main reason that offline studies, like the Retrospective U.S. Land Data Assimilation System (LDAS) Project reported in this paper, or LDAS in general, are taking place on both regional domains [North American LDAS (NLDAS); Mitchell et al. 2004a; Maurer et al. 2002; European LDAS (ELDAS); van den Hurk et al. 2002] and global domains [Global LDAS (GLDAS); Rodell et al. 2004].

In recent years, with support from the Global Energy and Water Cycle Experiment (GEWEX) Continental-Scale International Project (GCIP), the Retrospective U.S. LDAS Project reported here was conducted at the National Oceanic and Atmospheric Administration (NOAA)/NCEP Climate Prediction Center (CPC), collaborating with the NOAA/NCEP Environmental Modeling Center (EMC), and implicitly profiting from all previous NLDAS efforts (Mitchell et al. 2004a). The Retrospective U.S. LDAS Project is part of an effort to upgrade NCEP CPC's system for monitoring and predicting U.S. soil moisture and associated land surface variables by replacing the current leaky bucket model (H96) with the more advanced Noah land surface model (LSM; Mitchell et al. 2004a; Ek et al. 2003). The multilayer Noah LSM allows one to monitor the vertical profile of soil moisture anomalies, as well as snowpack, thus providing two new degrees of freedom for

characterizing the severity of a drought, unlike drought monitors constructed around the CPC leaky bucket model. A similarly long and detailed land reanalysis has been made (Maurer et al. 2002) with the variable infiltration capacity (VIC) land surface model (Liang et al. 1994).

In addition to the choice of the land model (e.g., Noah or VIC), the quality of a long retroactive run is largely dependent on the forcing datasets. In total, we need to prescribe temperature, humidity, wind speed, surface pressure, solar and infrared downward radiation, and precipitation in order to run the Noah model properly. Ideally, one wants the best possible datasets (observations) for as long as possible at as high as possible a resolution. But for several variables there is no such data, at least not very far back. We opted to extract all variables from NNGR, except for precipitation, which is derived from gauges. The length of time over which NNGR is available dictates that we cannot start any earlier than 1948, which is a setback from the CPC leaky bucket that started in 1931 (H96). If one wants a long dataset for climatological applications there are hardly any alternatives to using NNGR, which has its own problems and will be discussed later. We note that for the VIC retroactive run Maurer et al. (2002) derived forcing from a few measured variables that do exist, such as empirically linking radiation to the difference of maximum and minimum temperatures. Here we follow an approach that instead leverages the NNGR gridded analyses at NCEP.

A word of caution on the resolution is in order. While we utilize the standard NLDAS 1/8° grid, the forcing datasets, especially those derived from global reanalysis (a 6 h, T62 Gaussian grid), are not really at the resolution of NLDAS (an hourly, 1/8° grid). Rather, they are interpolated larger-scale fields, though adjusted for the NLDAS terrain [section 2b(1)]. Most of the smaller-scale details that appear in the output thus are most likely related to the precipitation and prescribed soil, vegetation, and (especially) orographic properties.

Therefore, the main effort of the Retrospective U.S. LDAS Project is to derive a viable dataset of surface meteorological forcing to rerun the Noah land surface model retroactively as far back as possible (1948–present), thus essentially providing a "land reanalysis." It is expected that the output of the Retrospective U.S. LDAS Project will provide more temporally self-consistent and spatially detailed and improved land surface datasets over multidecadal time periods.

The purpose of this paper is to describe the 51-yr retrospective U.S. land reanalysis using the Noah land surface model. It is organized as follows: in section 2, we describe the Noah land surface model and the 51 yr of hourly input forcing and land surface outputs; in section 3, we present preliminary results for validating and analyzing the ability of the Noah land surface model to simulate the observed annual cycle and interannual variability of soil moisture, as well as the annual cycle of U.S. land surface water and energy budgets; the conclusions and discussion from this study are provided in section 4.

2. Model and forcing data

a. Noah land surface model and land surface characteristics

Since the late 1990s, one of the several LDAS land surface models, the Noah LSM, has been run at EMC/NCEP in a real-time forward mode. The Noah LSM originated from a physically based surface–vegetation–atmosphere transfer (SVAT) scheme (Mahrt and Pan 1984). During the past 10 yr, the Noah LSM underwent substantial upgrades, including an increase of the number of soil layers, and modifications to the formulations of canopy conductance, bare soil evaporation, vegetation phenology, ground heat flux, surface runoff and infiltration, thermal roughness length in the surface layer exchange coefficients, and snowpack physics (Ek et al. 2003; Mitchell et al. 2004a). These model enhancements significantly improve the performance of the Noah LSM. The new Noah LSM simulates both liquid and frozen soil moisture, soil temperature, land surface skin temperature, snowpack water equivalent and snowpack density, canopy water content, and the energy and water fluxes of the land surface energy and water balances. In various coupled and uncoupled assessments, the Noah LSM has been proven to have the ability to reproduce the observed land surface energy and water budgets quite effectively (Mitchell et al. 2004a; Ek et al. 2003).

The Noah LSM has four vertical soil layers, with the root zone spanning the top three (four) layers for nonforest (forest) vegetation classes. The four default soil layers have constant thicknesses of 10, 30, 60, and 100 cm, yielding a total depth of 2 m. The Noah LSM was configured on the NLDAS grid, having dimensions of 464 × 224 at 0.125° × 0.125° resolution spanning a domain bounded by 25.0625°–52.9375°N, 67.0625°–124.9375°W. On this grid, the elevation was derived by averaging the 1-km digital elevation of the U.S. Geological Survey (USGS) GTOPO30 database (Verdin and Greenlee 1996). The vegetation classification was derived from the global, 1-km, Advanced Very High Resolution Radiometer (AVHRR)-based, 13-class vegetation database of Hansen et al. (2000). The 16-class

soil texture database was derived from the top layer of the 1-km, 11-layer State Soil Geographic (STATSGO) database of Miller and White (1998). The monthly fraction of green vegetation is taken from the satellite-based [National Environmental Satellite, Data, and Information Service (NESDIS) AVHRR] 5-yr global monthly climatology of green vegetation fraction (Gutman and Ignatov 1998).

Further details on the NLDAS configuration are given in the forerunner NLDAS study of Mitchell et al. (2004a), which for a 3-yr period rich in observations for validation (from 1 October 1996 to 30 September 1999) assesses a retrospective NLDAS run with four land models [Noah, VIC, Mosaic, and Sacramento (hereafter SAC)] executed with common hourly surface forcing and streamflow routing on the 1/8° NLDAS grid described above. In that study, the validation of energy and water budgets, soil moisture, soil temperature, streamflow, snowpack, etc., showed large intermodel differences, and the degree of agreement between the models and observations varied by the model and the quantity being verified. For the mean annual water budget, the results from the Noah LSM were the closest to the observations, while a high (low) bias in evaporation and low (high) bias in runoff was evident in Mosaic and SAC (VIC). When compared with Illinois 2-m soil moisture observations, both Noah and SAC agreed with the observations in storage range and magnitude, while VIC showed a good storage range but low magnitude and Mosaic showed a high storage range. Additionally, the simulated daily mean 0–40-cm soil moisture changes of the four models were verified with the spatially averaged 72-station data of the Oklahoma Mesonet, and clear differences were again found among the models and between the models and observations, with VIC showing the best results. The simulated snowpack water equivalent (SWE) at mountain snow telemetry (SNOTEL) sites also showed large differences among the models, with VIC and SAC yielding the smallest bias in simulated SWE and regional snow cover, and VIC giving the best snowmelt timing. Validation of surface energy fluxes over the U.S. Southern Great Plains (SGP) showed that overall Noah had the smallest bias. Because Noah, VIC, Mosaic, and SAC were not tuned or calibrated in NLDAS, the above model intercomparisons are preliminary and must not be viewed as a ranking of the models.

b. *Forcing dataset for the Retrospective U.S. LDAS Project*

To run the Noah LSM retrospectively for 50+ years, the quality of the forcing dataset will greatly impact the output of the land surface model and thus is critical for this project. It is well known that we lack long-term records for the observational radiation data (either satellite estimation or ground observation) over large areas, especially at 1/8° resolution. At the present time, a viable and temporally self-consistent source of all seven required surface atmospheric variables over 50+ years is from NNGR, which NCEP is also extending operationally in real time. Prior assessment of NNGR (Berbery et al. 1999; J. Huang 2001, personal communication) has found that there is a positive bias in the NNGR downward surface shortwave radiation, as well as a negative (albeit smaller) bias in the NNGR downward surface longwave radiation. Because the Noah LSM takes the downward surface shortwave radiation and downward surface longwave radiation in the form of the total incoming radiation forcing, we decided not to do any bias correction for either of them.

As the first step of the project, a 51-yr (1948–98) hourly forcing dataset was generated on the 1/8° NLDAS grid, namely, 2-m air temperature (T_a) and humidity (q), surface pressure (p_*), 10-m wind speed $(u^2 + v^2)^{1/2}$, surface downward shortwave radiation (S↓), and surface downward longwave radiation (IR↓) from NNGR. The hourly and daily precipitation datasets are taken from CPC (Higgins et al. 2000, 2004) and NOAA's Office of Hydrologic Development (OHD) (J. Schaake 2001, personal communication). The input precipitation is the total precipitation, disregarding whether it is frozen or unfrozen. A schematic of the input and output from the Retrospective U.S. LDAS Project is shown in Fig. 1.

To make a homogeneous forcing dataset at the required spatial and temporal resolutions, some unique procedures and techniques were developed to prepare this hourly and high-resolution retroactive forcing dataset. The details are provided next.

1) PREPARE ATMOSPHERIC FORCING

The procedures for creating atmospheric forcing from NNGR are as follows.

1) Extract seven variables (T_a, q, p_*, u, v, $S\downarrow$, IR↓) from the NNGR dataset (which is taken 4 times daily at 0000, 0600, 1200, and 1800 UTC, from 1948 to1998); here T_a, q, p_*, u, and v are instantaneous variables and $S\downarrow$, IR↓ are 6-h averages.
2) Convert data from the T62 NNGR Gaussian grid to the 1/8° NLDAS grid using bilinear interpolation.
3) Interpolate 6-h data to hourly data using linear interpolation, except for T_a and S↓ (see procedures 4, 5, and 6).
4) Process surface downward shortwave radiation $S\downarrow$ by linearly interpolating the 6-h mean data to gen-

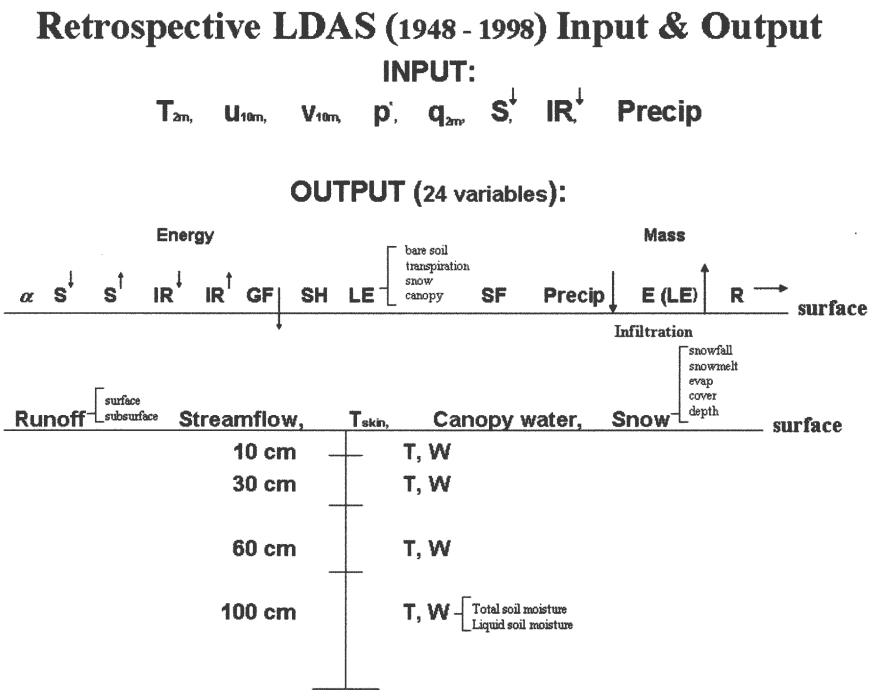

FIG. 1. Schematic of the input and output of the Retrospective U.S. LDAS Project. Most variables are described in the paper.

erate $S\downarrow$ every 3 h. Then, based on the information of location (latitude and longitude) and time (hour and date), apply a solar zenith angle diurnal adjustment to disaggregate the $S\downarrow$ to the needed hourly time step. This produces a more accurate diurnal solar cycle than does a simple linear interpolation.

5) Determine the hourly temperature from (a) the 6-hourly temperature (the "boundary values," 4 times daily) and (b) the NNGR 6-hourly maximum and minimum temperature ($T_{\max}$ and $T_{\min}$) for each 6-h interval (allowing for an error in the $T_{\max}$ and $T_{\min}$ data that was stored). The time of the maximum and minimum are not given, so their times can only be known for sure when the maximum and minimum coincide with the boundary values. If this was not the case, we drew straight lines from the boundaries to the maximum and minimum, situating the maximum and minimum where it seems most reasonable (given the local time). In doing so we also had to account for a coding error[1] in the NNGR.
6) Perform an elevation adjustment to 2-m air temperature, surface pressure, downward longwave radiation, and 2-m specific humidity, as in the 1996–99 NLDAS project (Cosgrove et al. 2003a). Figure 2 shows significant surface elevation differences between NNGR and NLDAS, especially in the western mountain areas. The detailed procedures for the elevation adjustments for the four variables can be seen in appendix A.

2) PREPARE PRECIPITATION FORCING

There are three precipitation datasets used here: CPC/OHD daily precipitation (which was developed in support of the North America Regional Reanalysis and the present project, but is only available for the conterminous United States), CPC daily unified precipitation, and CPC hourly precipitation. We mainly use the first and third. For the small areas inside the NLDAS but outside the conterminous United States, the CPC daily unified precipitation is used.

The newly improved CPC/OHD daily precipitation over 1948–98 is different from the CPC daily unified precipitation (Higgins et al. 2000, 2004) in the following respective ways: (a) a terrain adjustment using the Parameter-elevation Regressions on Independent Slopes Model (PRISM; which uses historical gauge measurements of precipitation and a digital elevation model to generate estimates of annual, monthly and event-based climatology; Daly et al. 1994), only available for the conterminous United States, versus no terrain adjust-

[1] Extremes were not zeroed out at the beginning of the 6-h interval, but 1 h off. As a result of this coding error in global reanalysis, the recorded maximum and minimum values are sometimes incorrect.

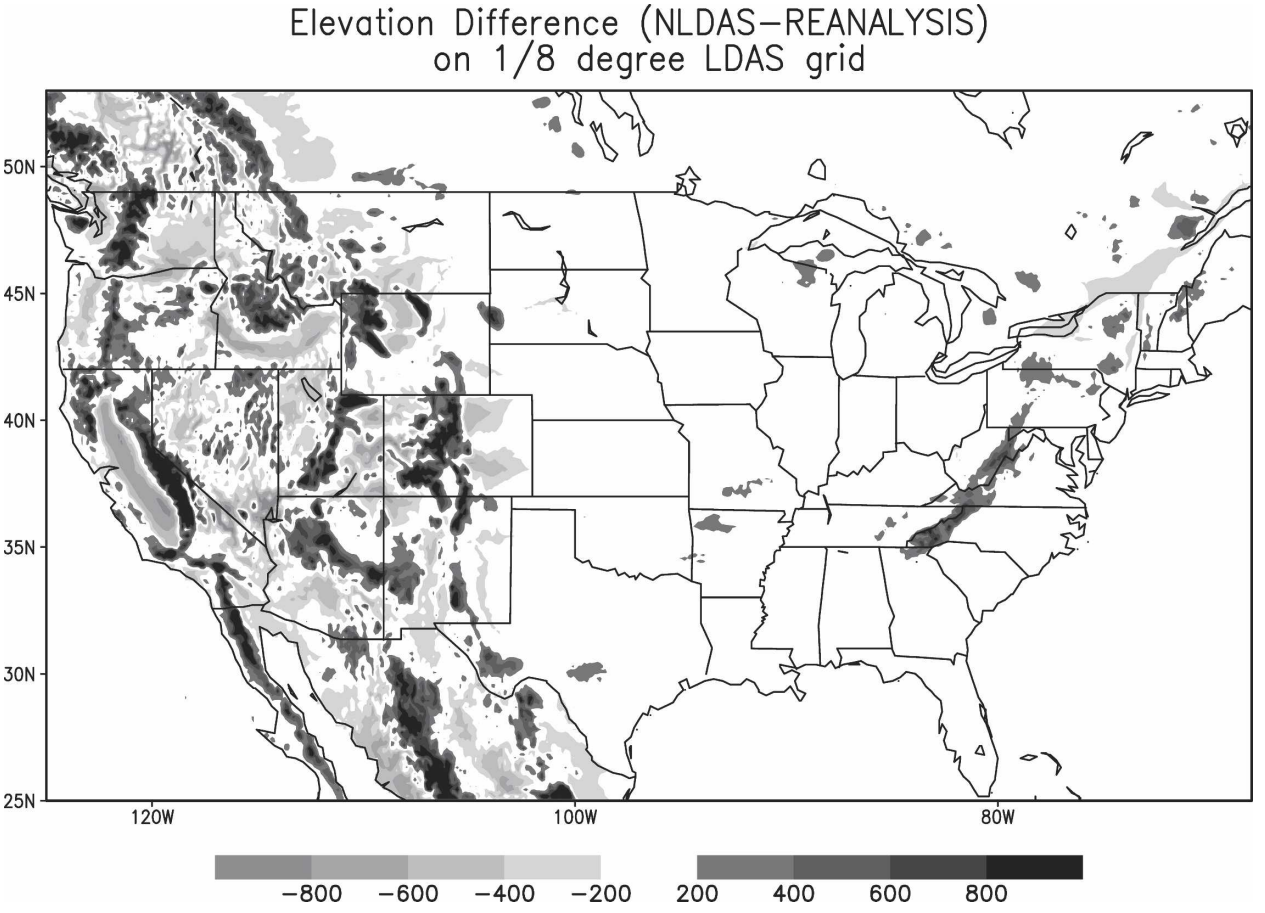

FIG. 2. Surface elevation difference between the 1/8° NLDAS topography and the NCEP–NCAR Global Reanalysis topography interpolated to the 1/8° NLDAS grid. Unit: m.

ment, (b) least squares distance weighting as the objective analysis scheme versus a modified Cressman analysis scheme, and (c) on the 1/8° U.S. LDAS grid versus a 1/4° grid. The CPC hourly precipitation dataset, which is a Cressman-based analysis, also was used here, but only to generate temporal disaggregation weights. The hourly precipitation analysis uses about 2900 gauges on a 2.5° × 2.0° grid, while the daily precipitation analysis uses about 11 000 gauges on the 0.125° × 0.125° NLDAS grid. The approach here is to use the high temporal resolution hourly precipitation analysis to derive weights to temporally disaggregate the high spatial resolution daily precipitation analysis to obtain an hourly high temporal–spatial resolution precipitation analysis. The detailed procedures for creating such a precipitation forcing are as follow:

1) Use linear temporal interpolation and extrapolation to fill in any missing values in the CPC hourly precipitation analysis. The missing values are around 0.2% of the total hourly data and they often happened in the first few hours at the very beginning of the years.
2) Calculate the hourly weights from the CPC hourly precipitation analysis on the 2.5° × 2.0° grid, then interpolate the weights to the 0.125° × 0.125° NLDAS grid.
3) Apply the hourly weights to the daily precipitation analysis on the 0.125° × 0.125° NLDAS grid to obtain the hourly high spatial and temporal resolution precipitation on the 0.125 ° × 0.125° NLDAS grid.

Because the hourly observations are substantially fewer at many grid points than those of daily observations, it is possible that there are places where a daily summation of hourly precipitation is zero (then the hourly weights are zero, too), but the daily precipitation is nonzero. In this case, if nearby places have nonzero hourly weights, those weights are used for these places. Otherwise, a uniform hourly weight, that is, 1/24, is used to generate the hourly precipitation from daily precipitation.

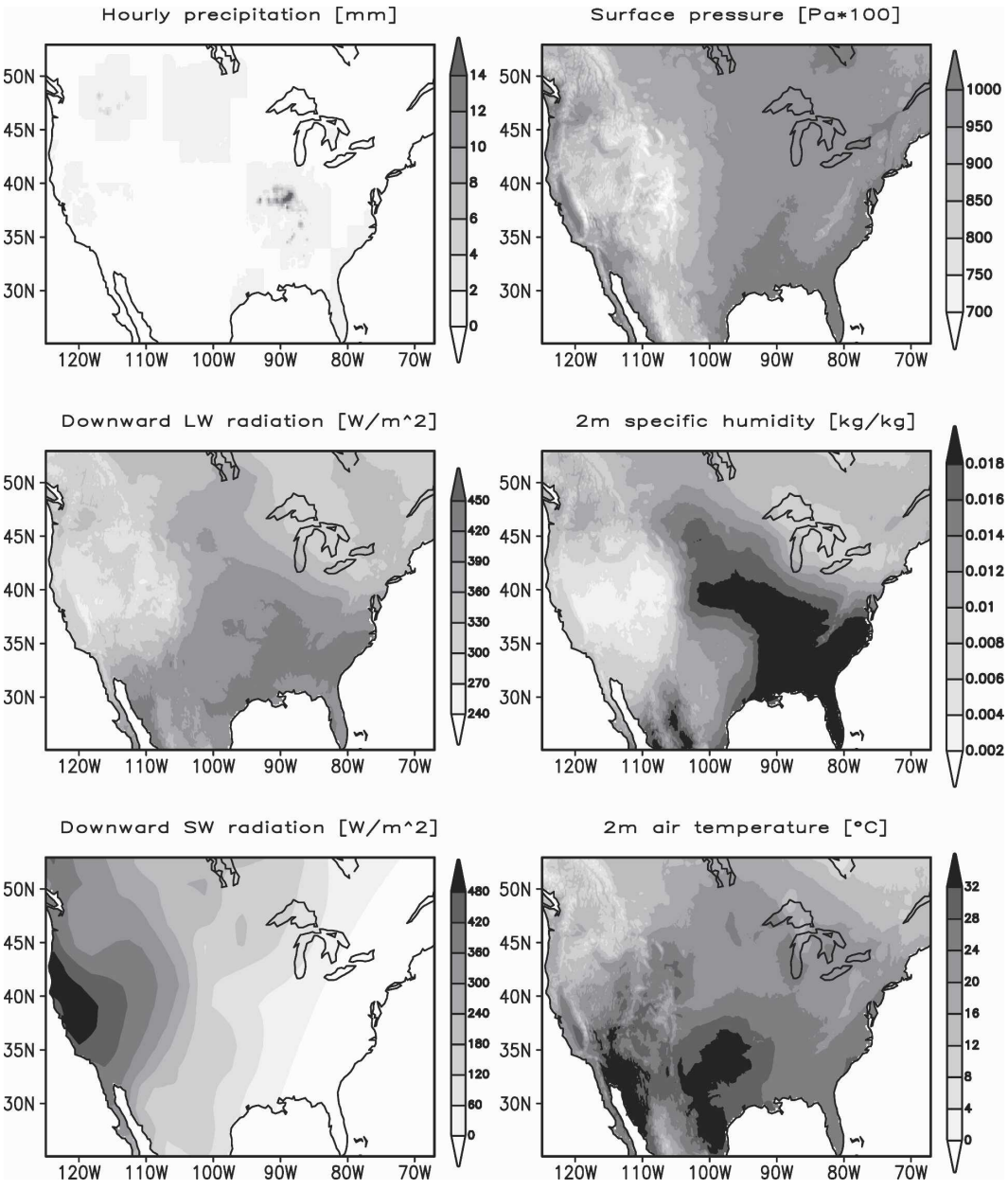

FIG. 3. The hourly forcing fields (P, IR$\downarrow$, $S\downarrow$, p_*, q, T_a) valid at 0100 UTC 16 Jul 1993, as examples of spatial resolution of the retrospective NLDAS forcing data (wind speed forcing not shown).

After the hourly precipitation and atmospheric forcing are created, they are merged and organized in an hourly file in gridded binary (GRIB) format—a widely used standard for gridded fields at major NWP centers such as NCEP. The size of the tarred and compressed forcing data files is around 6 GB yr^{-1}. Figure 3 depicts characteristics of the retrospective forcing data. The data for 0100 UTC 16 July 1993 is chosen as an example. One can see detailed structures in five of the six maps, especially the orographic effects. In the case of surface downward solar radiation, hardly any small-scale features are seen. This 51-yr set of hourly high-resolution surface forcing is valuable and may also be used for other models or for modeling comparison purposes.

c. Running the model

The Noah LSM used for the retrospective U.S. LDAS run is executed with a 15-min time step for reasons of numerical robustness, physical (especially diurnal) realism, and compatibility with coupled applica-

TABLE 1. Energy balance components. Avg: average.

Definition	Variable	GRIB no.	Positive	Unit	Type
Net surface shortwave radiation	NSWRS	111	Upward	W m^{-2}	Avg
Net surface longwave radiation	NLWRS	112	Upward	W m^{-2}	Avg
Latent heat flux	LHTFL	121	Upward	W m^{-2}	Avg
Sensible heat flux	SHTFL	122	Upward	W m^{-2}	Avg
Ground heat flux	GFLUX	155	Upward	W m^{-2}	Avg
Snow phase change heat flux	SNOHF	229	Liquid to solid	W m^{-2}	Avg
Downward surface shortwave radiation	DSWRF	204	Always	W m^{-2}	Avg
Downward surface longwave radiation	DLWRF	205	Always	W m^{-2}	Avg

tions in atmospheric prediction models. Therefore, the hourly forcing data are further interpolated linearly to 15-min intervals in the LSM driver. Before starting the Retrospective U.S. LDAS Project, proper initialization of the Noah LSM is important. Cosgrove et al. (2003b) estimate the spin-up characteristics of the NLDAS system and find the practical spin-up time for NLDAS system is about 1 yr. The spinup is also temporally and spatially dependent. Some finescales may take a much longer time to reach equilibrium. Our studies have similar results. Therefore, in order to reduce spin-up time, the initial conditions for this retrospective project were taken from an operational NLDAS run (1 July 1998) from EMC/NCEP, which started in October 1996. By choosing to start in the summer, we avoid largely the difficult of cold-season initialization. We set the "time stamp" back to 1 July 1948 and then repeatedly ran the Noah LSM with the 1948 forcing for 3.5 yr to overcome the bulk of the spinup. Then, we started the retrospective U.S. LDAS run from 1 January 1948 and executed forward to 31 December 1998.

d. Outputs of the retrospective U.S. LDAS project—Data format and categories

The retrospective U.S. LDAS dataset is generated at the 1/8° NLDAS grid and all of the results are stored in either binary or GRIB format. Table 1 and Table 2 give more detailed information for these available variables, and a more detailed description for the data structure can be found in appendix B. All of the above forcing data and the full land reanalysis dataset from the Retrospective U.S. LDAS Project are archived on the NCEP IBM High-Performance Storage System (HPSS). Users having accounts on the NCEP IBM computers can easily access these datasets. Another copy of this dataset will be archived at NCAR in the near future.

3. Preliminary analysis

a. Data validation against Illinois soil moisture

The Illinois network of soil moisture observations provides one of the few long-term time series of routine

TABLE 2. Water balance components, and surface and subsurface state variables. Acm: accumulation, ins: instantaneous, and avg: average.

Definition	Variable	GRIB no.	Positive	Unit	Type
Snowfall (frozen precipitation)	ASNOW	131	Always	Kg m^{-2}	Acm
Rainfall (unfrozen precipitation)	ARAIN	132	Always	Kg m^{-2}	Acm
Total evaporation (all source)	Evp	057	Upward	Kg m^{-2}	Acm
Surface runoff	SSRUN	235	Exit grid box	Kg m^{-2}	Acm
Subsurface runoff	BGRUN	234	Exit grid box	Kg m^{-2}	Acm
Snowmelt	SNOM	099	Solid to liquid	Kg m^{-2}	Acm
Skin temperature	AVSFT	138	Always	K	Ins
Snow-water equivalent	WEASD	065	Always	m	Ins
Plant canopy surface water storage	SSTOR	223	Always	Kg m^{-2}	Ins
Soil temperature in four layers	SOILT	085	Always	K	Ins
Soil moisture in four layers	SOILM	086	Always	Kg m^{-2}	Ins
Liquid soil moisture in four layers	LSOIL	151	Always	Kg m^{-2}	Ins
Potential evaporation	PEVPR	145	Always	W m^{-2}	Avg
Snow depth	SNOD	066	Always	m	Ins
Snow cover	SNOC	238	Always	%	Ins
Snow evaporation (sublimation)	SBSNO	173	Upward	W m^{-2}	Avg

soil moisture observations in the United States (Hollinger and Isard 1994). This dataset consists of soil moisture measured at 18 sites throughout the state of Illinois from 1981 to the present, measured with the neutron-probe technique calibrated with gravimetric observations. The data are observed a few times each month, and are measured for the top 10 cm of soil and then for 10 layers (e.g., 0–10, 10–30, 30–50 cm, . . . 170–190, 190–200 cm) down to a depth of 2 m. The vegetation at all stations is grass, except for one station with bare soil measurements, which is at the same location as a grass-covered station. The dataset is available from the Global Soil Moisture Data Bank (Robock et al. 2000) and is used here to verify the ability of the Noah LSM to simulate the annual mean, seasonal cycle, and interannual variability of soil moisture in the upper 2 m of the soil column (both the 2-m integral and vertical profile). Following Schaake et al. (2004), only 17 sites are used in this study because data from one of the 18 sites is quite different from that of the other 17. Although the spatial and temporal resolutions of the observed Illinois soil moisture data are not compatible with those from the Retrospective U.S. LDAS Project, this dataset is the best dataset we have to validate this long retrospective LDAS run.

The seasonal cycle and interannual variability of the observed and simulated monthly averaged soil moisture in the 2-m column for the period from January 1984 to December 1998 in northern, central, and southern Illinois are shown in Fig. 4. The model results are spatially averaged over all grid points inside three rectangular regions, nominally representing northern, central, and southern Illinois at 41°–43°N, 90°–88°W; 39°–41°N, 90°–88°W; and 37°–39°N, 90°–88°W, respectively. The observed results are averaged from five northern stations, five central stations, and seven southern stations, respectively. We remind readers that the forcing is on the 1/8° NLDAS grid, not the point-wise local forcing of the 17 stations.

In Fig. 4, for northern Illinois, the time evolution of the simulated anomalies of the 2-m column soil moisture follows the observations quite well and most wet and dry events are captured very well. However, exceptions can be seen, such as the 1994 dry event. The phase of the seasonal cycle of the model 2-m column soil moisture is also well simulated (a big improvement over CPC's leaky bucket model), but in the mean the simulation is wetter than the observations by about 50 mm. Similarly, in central Illinois the wet and dry events and the evolution of the simulated anomalies of the 2-m column soil moisture follow the observations reasonably well. Compared with the observations, the simulated annual mean soil moisture is still too wet, now by about 30 mm. For southern Illinois, the anomalies and annual cycle of the simulated 2-m column soil moisture almost perfectly reproduce the observations, not only in the temporal phases, but also in the amplitude of variations and the annual mean. The anomaly correlations between the observed and Noah LSM–simulated soil moisture are 0.71, 0.80, and 0.75 for the above three Illinois regions. The anomaly correlations between the observed and CPC leaky bucket model (H96) simulated soil moisture in the same period are 0.70, 0.72, and 0.55. The Noah LSM shows improvement of simulated soil moisture not only in the phase of the annual cycle (which is poor in CPC's leaky bucket model, see Fig. 1 in Van den Dool et al. 2003), but also to a lesser degree in the interannual variability, especially in central and southern Illinois.

In contrast to most of the previous studies, we can now validate vertical profiles against Illinois observations. The simulated monthly soil moisture (averaged statewide) in the four individual model layers and the observed monthly soil moisture (averaged from 17 stations) in the corresponding layers over Illinois are shown in Fig. 5. The anomaly correlations between the observed and Noah LSM–simulated soil moisture at different model layers (from top to bottom) are 0.64, 0.72, 0.73, and 0.63, respectively. For the top-10-cm layer, the temporal phase of the variation of simulated soil moisture follows that of the observed soil moisture reasonably well. However, the amplitude of the simulated fluctuations of both the soil moisture anomalies and annual cycle is far smaller than those observed in all seasons. The LSM successfully captures most of the wet and dry events in the second model layer, but the model seriously underestimates the range of the observed soil moisture annual cycle. The timing of the observed soil moisture annual cycle in this layer is not simulated well, the maximum is 1 month early and the minimum is 1 month late. Further down to the last layer of the model root zone at 40–100-cm depth, the results are the best. Here the Noah LSM simulates the observed soil moisture in both amplitude and phase far better than in the upper two layers. But, the simulated annual mean is still slightly wetter than that of the observations. For the layer of the subroot zone at 100–200-cm depth (also see Fig. 6), the variability of the simulated soil moisture is actually larger than the observations and the timing of the minimum in the annual cycle is 1 month early, such that the results for the full 2 m on a monthly basis are very good (see Fig. 4), because of the compensating biases. We thus note that the integral of the simulated 2-m soil moisture masks problems in the vertical profile of the simulation.

Here we also report that the evolution of the ob-

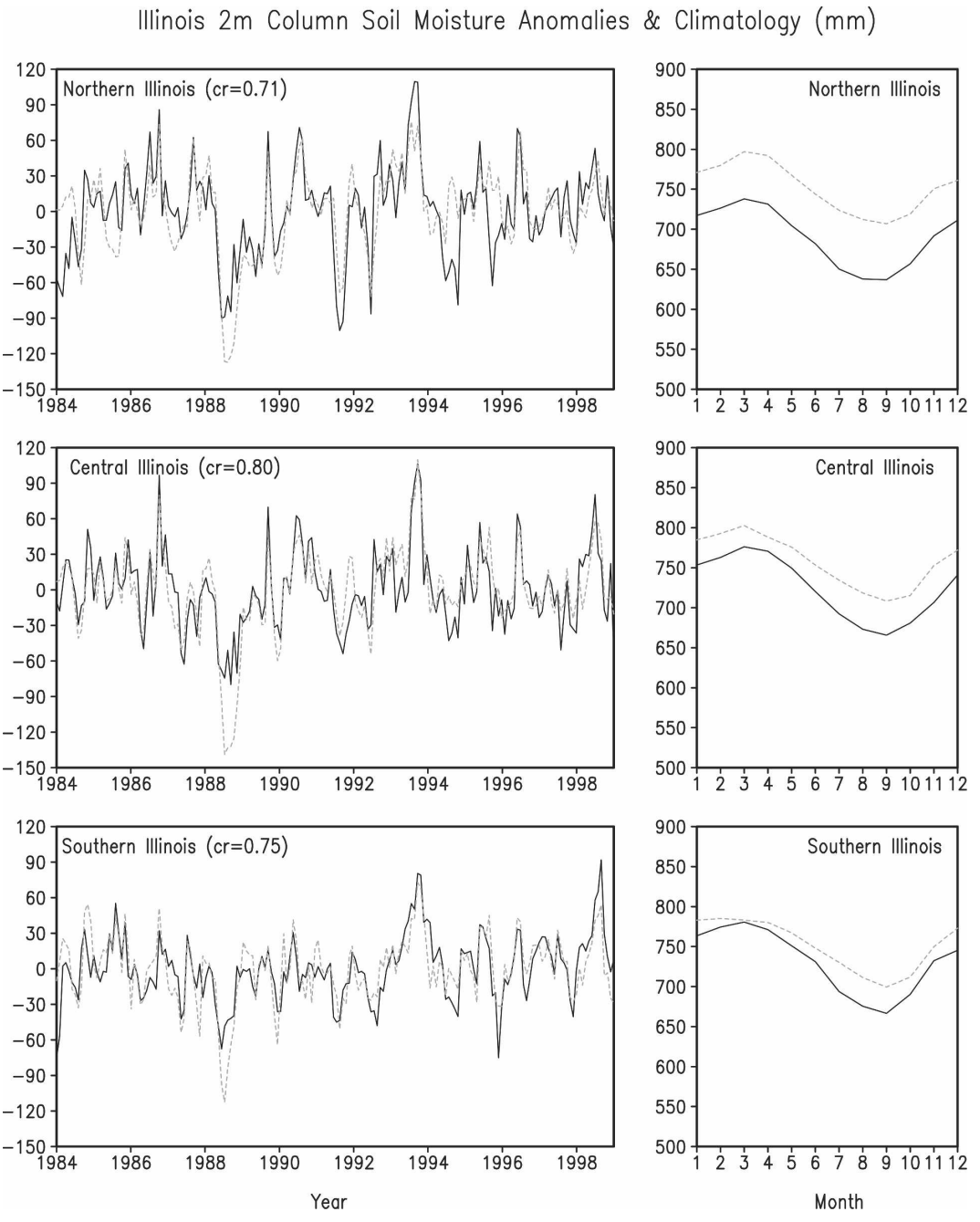

FIG. 4. The (right) mean annual cycle and (left) monthly anomalies of the observed (solid line) and simulated (dashed line) 2-m column soil moisture (mm) in northern, central, and southern Illinois from 1984 to 1998. The anomaly correlation is shown for each Illinois sector.

served Illinois soil moisture from 1981 to1983 is clearly different from the later observations. The calculated 10-yr running mean correlations from outputs of the Noah LSM and the CPC leaky bucket model (see information available online at http://www.cpc.ncep.noaa.gov/soilmst/sm_il.html) against the observed Illinois soil moisture display the same features—lower correlations when 1981–83 are included, and then increased correlations that hold steady. Because there are no clear precipitation changes found in this period and the land surface models are not changed, it may represent a deficiency in the observed data in the first 3 yr. Therefore, the discussion in this subsection will be restricted to data after 1983.

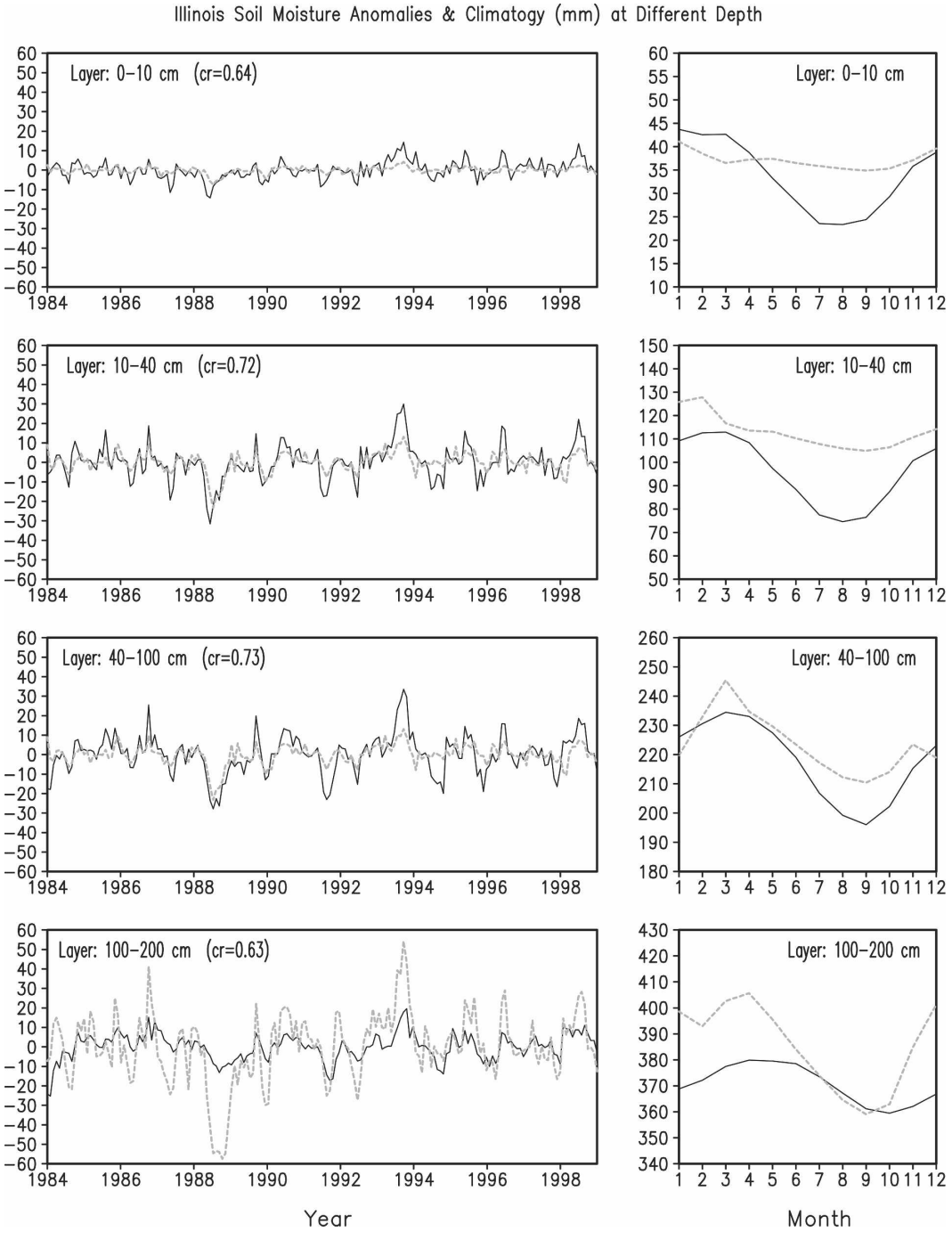

FIG. 5. The time evolution of the simulated monthly soil moisture (dashed line) in the four model layers and their corresponding observations (solid line, averaged from 17 stations) over Illinois from 1981 to 1998. The anomaly correlations are shown for each model layer.

The monthly time evolution of the observed and simulated soil moisture anomalies averaged over Illinois as a function of depth is shown in Fig. 6. To compare soil moisture anomalies for model and observation layers of unmatched depth, we express anomalies here as millimeters of water per 10-cm soil column. In general, the Noah LSM realistically captures most large dry and wet events down to the top 150 cm of the soil column. However, the Noah LSM tends to underestimate the observed soil moisture anomalies in the near-

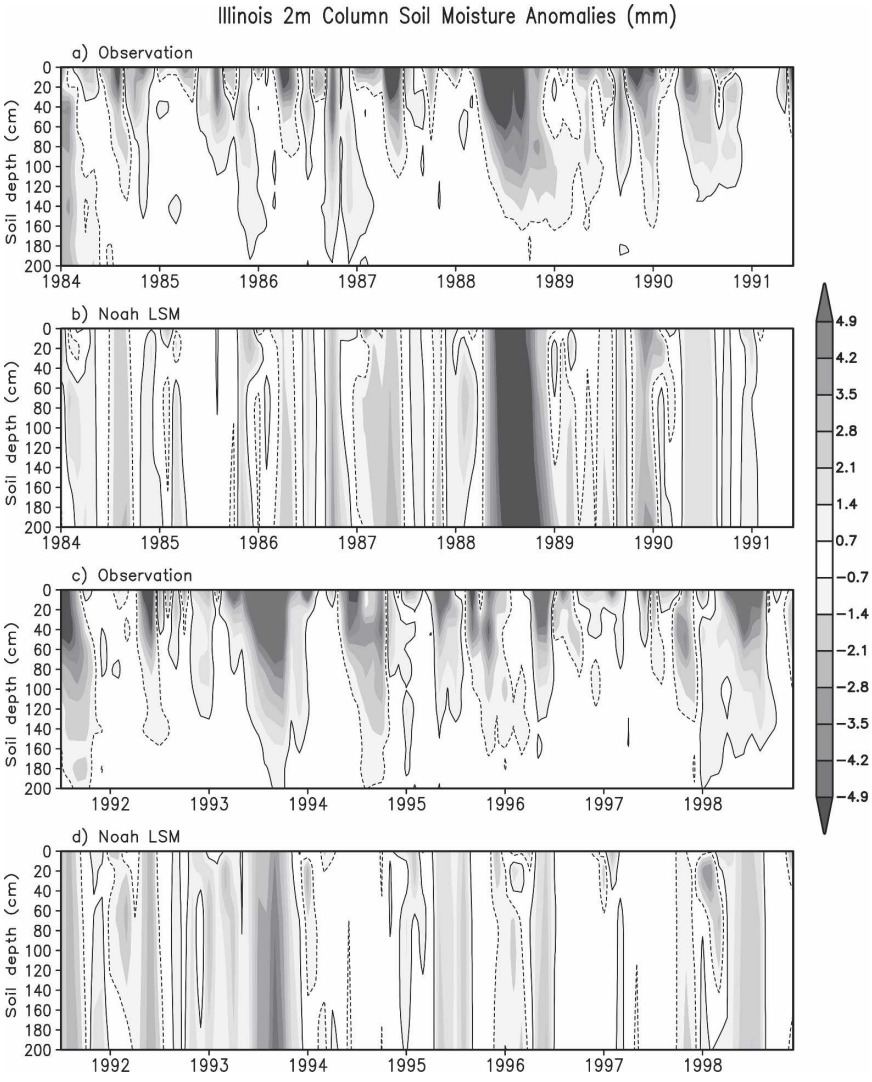

FIG. 6. Observed and simulated vertical distribution in top 2 m of soil moisture anomalies averaged over Illinois, as time series from January 1983 to December 1998. (a),(c) The simulations are from the four model layers: 0–10, 10–40, 40–100, and 100–200cm, and plotted at the center of each layer. (b),(d) The observations are derived from 0–10, 10–30, 30–50, 50–70, 70–90, 90–110, 110–130, 130–150, 150–170, 170–190, and 190–200 cm. The units are mm of water per 10 cm of soil.

surface layer and overestimate the observed soil moisture anomalies in deep model layers. The Noah LSM sometimes has difficulty in reproducing the slow downward propagation of the observed soil moisture anomalies. The differences between the observations and simulations are most likely because of model errors, but biases in the forcing data cannot be ruled out. These differences may suggest that the LSM needs more vertical layers in the top 150 cm of the soil column. Additionally, the Noah LSM assumes that the root density is uniform throughout the 1-m root zone throughout the growing season, in contrast to real conditions where root density generally decreases with depth and is less during the early growing season. The inconsistency in Fig. 6 may also be partly caused by the following inconsistencies of the two datasets: 1) spatial means: observations are averaged over 17 stations in Illinois and spatially averaged model data are calculated from 37°–43°N, 90°–88°W; 2) temporal means: the monthly observation data are based on the measurement interval of approximately every 2 weeks on average (less samples in cold season), and the model monthly means are calculated from daily mean data. Thus, more detailed studies are needed.

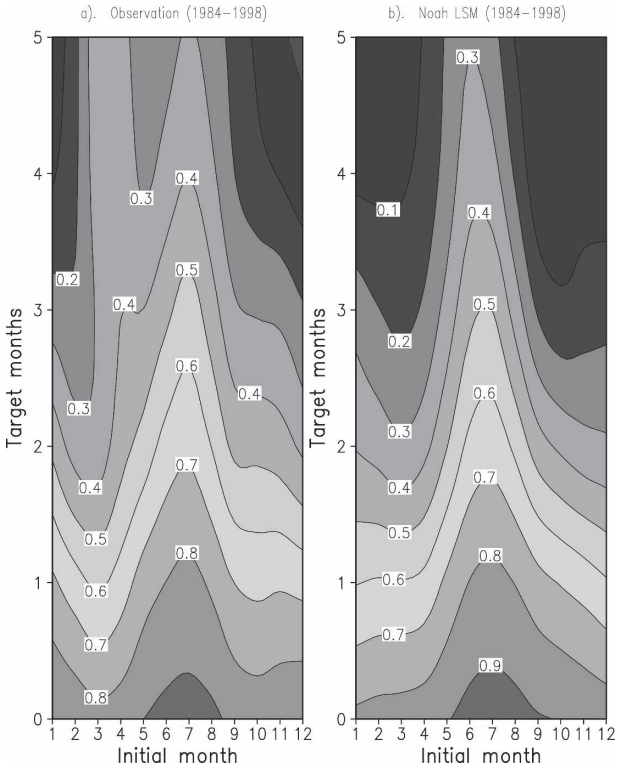

FIG. 7. Seasonal dependence of (a) observed and (b) simulated 2-m column soil moisture persistence (month-to-month autocorrelation) for 1984–98 over Illinois. The initial month is along the *x* axis, and the lead to the target month along the *y* axis.

The autocorrelation coefficient (ACC) of the 2-m column soil moisture as a function of the starting month (Fig. 7) shows that soil moisture persistence is seasonally dependent. The model results agree very well with the observations in both phase and amplitude. It shows that soil moisture has a rather strong persistence up to several months, with the largest persistence from July as the leading month and the smallest persistence in spring for the period of 1984–98. The simulated 2-m soil moisture persistence in 1951–80 (not shown) is different from that in 1984–98, with slightly larger persistence and its phase being different by about 2 or 3 months (with minimum in spring and maximum in late fall and early winter), which may indicate significant decadal climate change around late 1970s and early 1980s. The persistence of tropical SST in the mideast Pacific also has similar decadal change, with strong phase locking to the annual cycle before the 1970s and very little phase locking of persistence after the 1970s (Torrence and Webster 1998).

A similar calculation was done by using soil moisture from the CPC leaky bucket model. The results (not shown) reveal that simulated soil moisture persistence from the Noah LSM is better than that of the leaky bucket model in both phase and amplitude when compared with the observations for 1984–98.

b. Annual cycle of land surface water budget

The land surface water budget equation can be written as

$$\frac{dw}{dt} = P - E - R, \tag{1}$$

which depicts the balance between total surface water storage change (dw/dt) (w includes soil moisture, snowpack, and canopy water) and $P - E - R$, which includes total precipitation (P), total evaporation (E; from all sources, namely, evaporation of canopy interception, transpiration, evaporation from top soil surface, and sublimation from snowpack) and total runoff (R; surface runoff + subsurface runoff).

The January and July climatologies of all components of the land surface water balance, based on the data for 1961–90, are shown in Fig. 8. In general, on the continental scale, the land surface water storage change is positive (water recharged) almost everywhere in January, and negative (water depleted) in most areas (except the U.S. monsoon region and the southeastern United States) in July. Therefore, the maximum of soil moisture normally occurs in late winter and the minimum in late summer. For the precipitation, the West Coast states have a strong seasonal cycle, with a maximum in winter and minimum in summer. The Midwest and south-central regions also show a large change over the annual cycle. Evaporation depends strongly on air temperature and solar radiation and shows a pronounced seasonal cycle everywhere, with maximum in the warm season and minimum in the cold season, while the runoff is correspondingly opposite (as expected), with a maximum in the cold season and minimum in the warm season, except in mountain areas where the maximum runoff is associated with spring snowmelt, and Florida where runoff awaits the warm-season rains.

Figure 9 shows the seasonal variations of the $P - E - R$ climatology for January, April, July, and October. On average, the land surface water storage is recharged during the cold season and is depleted during the warm season. However, exceptions can be found in various places, such as the northern states (east of the Rocky Mountains to the Great Lakes), where snowmelt and late-spring rain play an important role in land surface water recharge in the spring. In the U.S. monsoon area, the land surface looses water in spring and recharges slightly in summer. In the southeast United States, the land surface water is depleted in spring and fall and recharged mainly in summer.

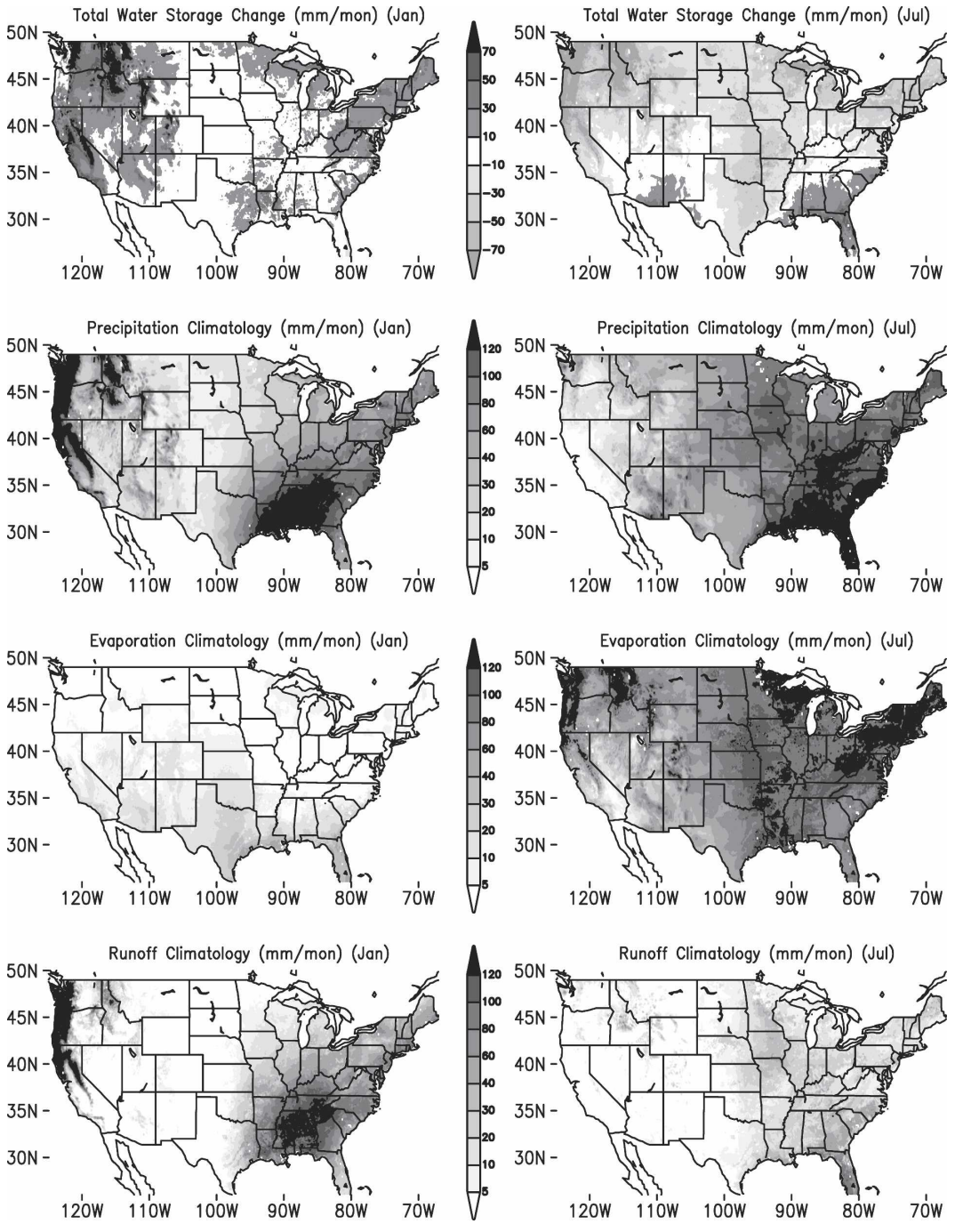

FIG. 8. (left) January and (right) July 1961–90 climatologies of all water balance components: (top to bottom) simulated total water storage change, observed precipitation, simulated evaporation, and runoff.

The annual cycle of the land surface water budget components and the water balance residual [i.e., $P - E - R - (dw/dt)$], averaged over the four U.S. quadrants for 1961–90, are shown in Fig. 10. In the northwestern, northeastern, and southeastern regions, although there are some differences in both the phases and amplitudes of the water balance components, the runoff is the most dominant component to balance precipitation in the cold season, peaking in early spring, while evaporation is the most dominant component to balance precipitation in the warm season. In the southwestern region, the precipitation, evaporation, and runoff are relatively

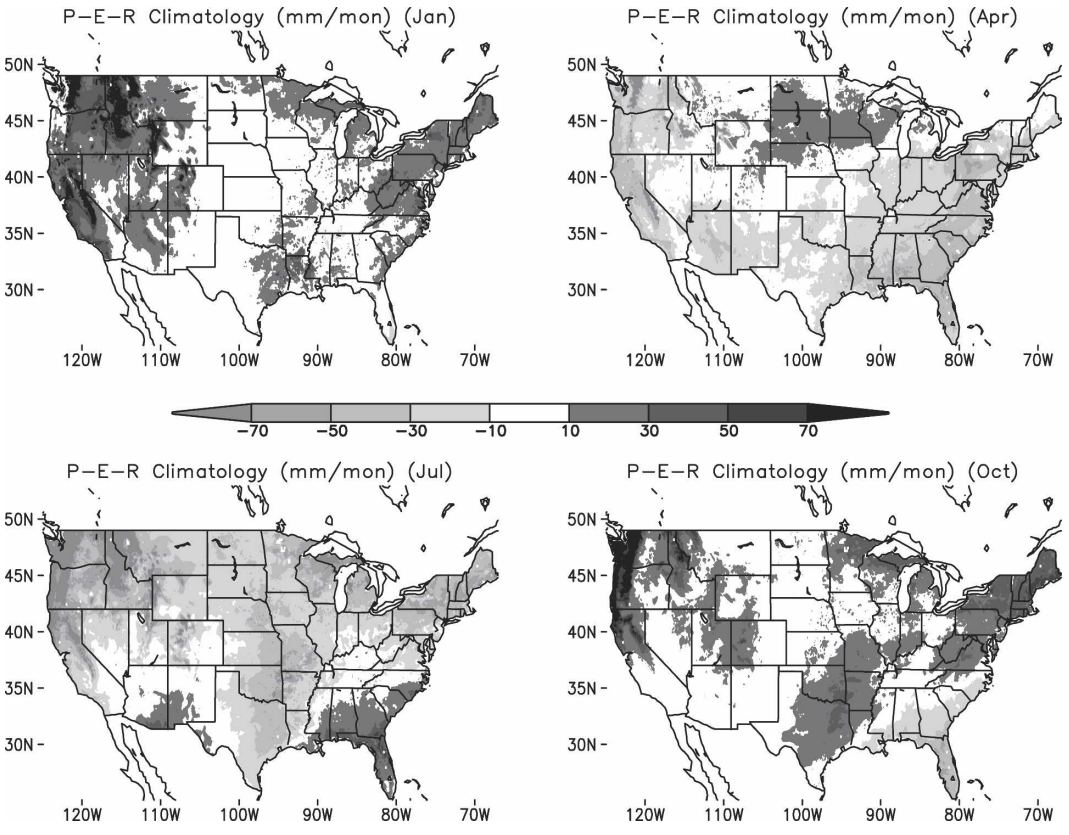

FIG. 9. Monthly climatology of $(P - E - R)$ over the conterminous United States for 1961–90 for the four midseason months. Monthly $P - E - R$ is approximately equal to the monthly change in the total surface water storage change $[(dw/dt)]$. Units: mm month^{-1}.

small all year-round. The water budget in the southwestern region largely depends on the balance between the precipitation and evaporation. It was found that the water balance residual is quite small most of time.

Table 3 provides the simulated partitioning of mean annual precipitation into mean annual evaporation and runoff for the four U.S. quadrants for the 40-yr period of 1959–98. The results in Table 3 are very similar to the results of Fig. 3 of Mitchell et al. (2004a) for the 2-yr period from October 1997 to September 1999 and are very close to the observed mean annual partitioning given in Mitchell et al. (2004a) for the northeastern and southeastern quadrants.

For the land surface hydrological cycle averaged over the conterminous United States (Table 4) for the period of 1961–90, the annual range of the 2-m column soil moisture is around 86 mm. To balance P, evaporation is high in summer while runoff is the highest in late winter. In general, for the continental scale, the land surface water is depleted during the warm seasons and recharged during the cold seasons. Therefore, soil moisture reaches its maximum in March and minimum in September. The upper-1-m layer represents most of the annual variation (60 mm), but the deeper layer also has a significant role (26 mm). On an annual averaged basis, the simulated land surface water budget for the conterminous United States is closed for the period of 1961–90.

c. Annual cycle of land surface energy budget

The land surface is a very important energy source for driving the overlying atmospheric circulation. Understanding energy partitioning at the land surface and its variability are not only important for the land surface water cycle and energy exchange, but are also important for weather and climate prediction. Typically, the land surface energy balance can be expressed as

$$\mathrm{RES} = R_n - \mathrm{LE} - \mathrm{SH} - \mathrm{GF} - \mathrm{SF}, \qquad (2)$$

in which RES is the energy balance residual and $R_n = (S^{\downarrow} - S^{\uparrow} + \mathrm{IR}^{\downarrow} - \mathrm{IR}^{\uparrow})$ is the surface net radiation; $S^{\downarrow}$, $S^{\uparrow}$, $\mathrm{IR}^{\downarrow}$, and $\mathrm{IR}^{\uparrow}$ are surface downward shortwave radiation, surface upward shortwave radiation, surface

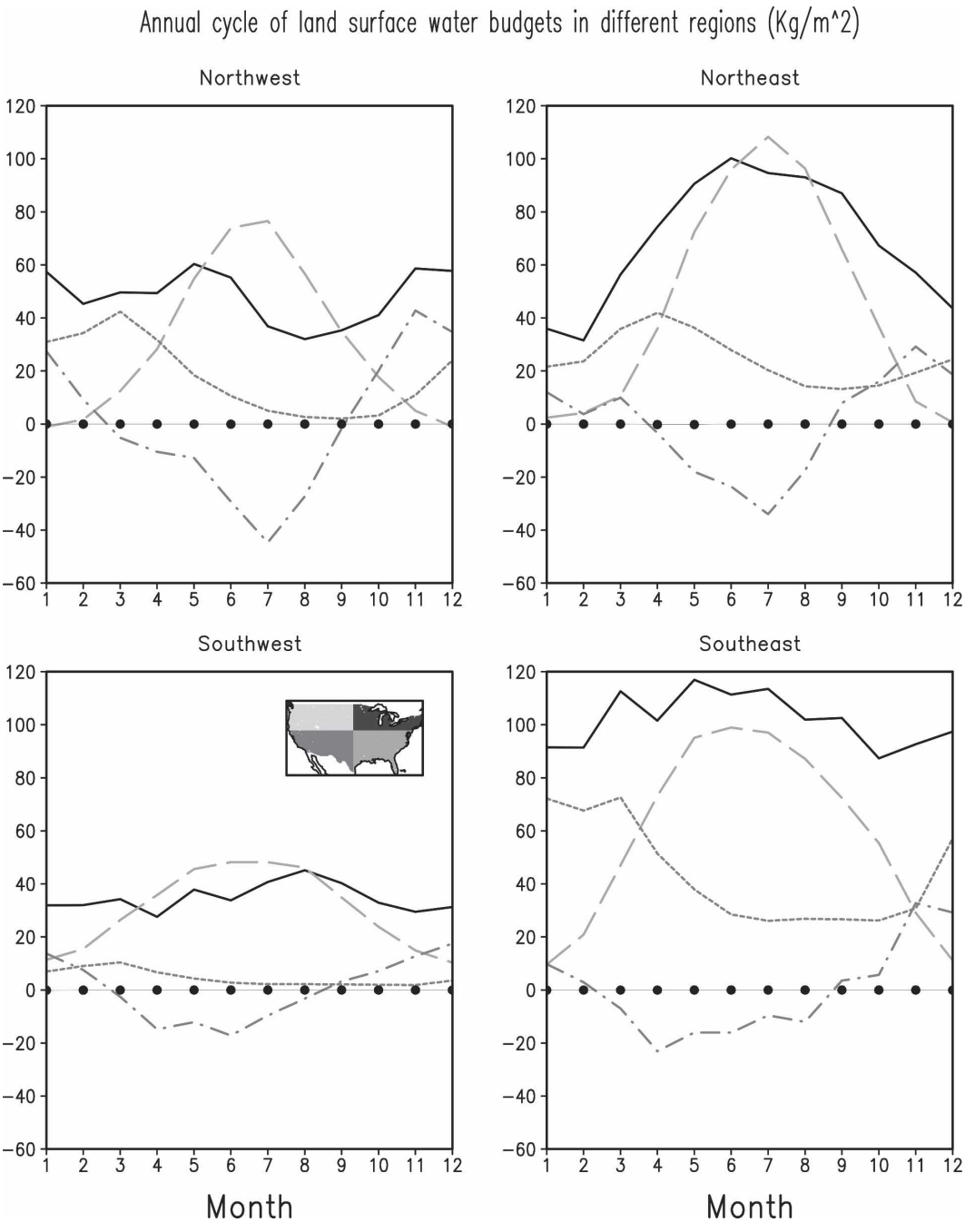

FIG. 10. The mean annual cycle of land surface water balance components [*P*: solid line, *E*: dashed line, *R*: dotted line, (*dw*/*dt*): dash-dotted line] and the residual (closed circle) for 1959–98 over the four U.S. subregions: northwest, northeast, southwest, and southeast (denoted by inset in lower-left panel).

downward longwave radiation, and surface upward longwave radiation, respectively, and LE, SH, GF, and SF are latent heat flux, sensible heat flux, ground heat flux, and snow phase change heat flux, respectively. By using the energy component definitions in Table 1, along with the sign conventions given therein, Eq. (2) can be written as

$$\mathrm{RES} = \mathrm{NSWRS} + \mathrm{NLWRS} + \mathrm{LHTFL} + \mathrm{SHTFL} - \mathrm{GFLUX} - \mathrm{SNOHF}. \quad (3)$$

In general, all energy components show clear seasonal changes in the four U.S. quadrants (Fig. 11). The surface net radiation (NSWRS + NLWRS) follows its seasonal course because of the sun–earth geometry.

TABLE 3. Partitioning of mean annual precipitation into mean annual evaporation and runoff for the four U.S. quadrants for 1959–98. Unit: mm yr^{-1}.

Region	P	E	R
Northwest	578	360	216
Northeast	831	538	293
Southwest	417	362	54
Southeast	1221	697	524

The seasonal cycle of the latent heat flux (LHTFL) and sensible heat flux (SHTFL) closely follow the seasonal course of the surface net radiation. During the warm season, the ground heat flux (GFLUX), which increases or decreases the ground energy storage, is negative, a monthly basis (downward, i.e., energy stored to ground), and opposite in the cold season. The snow phase change heat flux (SNOHF) is negative in the cold season and close to zero in the warm season. Most of the time, on a monthly mean basis, the incoming surface net radiation is largely balanced by the outgoing sensible heating and latent heating, while the ground heat flux and snow phase change heat flux are relatively small and only slightly modulate the balance. Ideally, the energy balance residual (RES) would be zero for long time average. The results here show that the monthly climatology of the energy balance residual is very small or close to zero.

Some unique features also can be seen in different regions, such as the relative contributions of sensible heat flux and latent heat flux (Bowen ratio B = SHTFL/LHTFL), which exhibits clear seasonal variation. For the northern states the incoming energy is mainly balanced by the sensible heating in the cold season, while during the warm season, latent heating and sensible heating are both important. In the southwestern region, sensible heating is the most dominant factor to balance net incoming radiative energy all of the time and latent heating is roughly half that of sensible heating. For the southeastern region, the sensible heating and latent heating are both important factors to balance the incoming energy, but their relative contribution changes with season; during the cold season, sensible heat is larger than latent heat, while the opposite holds in the warm season.

TABLE 4. U.S. monthly values of land surface hydrology components averaged over 30°–48°N, 125°–75°W. Units: mm for 2-m column soil moisture W and values in () are for top 1-m depth; mm $month^{-1}$ for all other components.

Month	W	P	E	R	$P - E - R$
1	581.2 (294.2)	52.0	5.5	31.8	14.6
2	592.5 (304.0)	49.8	10.3	33.3	6.2
3	600.0 (308.8)	62.9	24.5	39.1	−0.7
4	595.6 (302.0)	59.4	42.8	30.2	−13.7
5	582.8 (289.8)	70.9	64.8	21.2	−15.1
6	564.6 (276.8)	66.2	75.7	14.2	−23.8
7	538.4 (260.1)	64.8	77.8	10.4	−23.5
8	520.1 (250.0)	62.2	67.6	9.0	−14.3
9	514.3 (248.3)	61.4	49.3	8.8	3.3
10	520.2 (253.3)	51.7	31.9	9.1	10.8
11	539.8 (266.8)	58.0	14.0	13.5	30.5
12	565.8 (282.6)	58.5	4.5	27.3	26.8
Year	559.0 (278.1)	59.8	39.1	20.7	0.0

d. Simulated extreme hydrologic events: 1988 drought and 1993 flood

Extremes in land surface hydrology, that is, droughts and floods, have major impacts on life, property, and economic activities. The large-scale U.S. 1988 drought and 1993 flood are main examples. Both of them were among the most costly natural disasters in U.S. history, and damages caused by each of them exceeded $20 billion. The simulated anomalies of the 2-m column soil moisture and runoff (surface runoff + subsurface runoff) in July 1988 and July 1993 provide a striking illustration of the extreme contrast in spatial distributions for these drought and flood events over the conterminous United States (Fig. 12). Serious negative soil moisture anomalies in June 1988 (not shown) and July 1988 cover most of the central-eastern United States, together with a lower runoff than average. For the summer of 1993, extremely large positive soil moisture anomalies can be seen in the northern states, and upper Mississippi and Missouri River basins, accompanied by strikingly high runoff anomalies over the region. The extreme 1993 event resulted in record flooding over the upper Mississippi and Missouri River basins.

e. Sensitivity to temporal disaggregation of precipitation

Ideally, the temporal resolution of perfect forcing data should have the same time resolution as that of the model-executed time step (15 min for Noah LSM). However, at the present time it is impossible to obtain the observations at such high temporal resolution over a large area. Because precipitation is one of the most important forcing fields for land surface data assimilation and the daily precipitation data used in this work are more accurate and have much more gauge data than the hourly precipitation data, it makes sense to disaggregate the daily precipitation to hourly resolution as realistically as possible, such as the method we used in section 2b (hereafter control run). Another simple way (as done in Maurer et al. 2002) is to use equal or

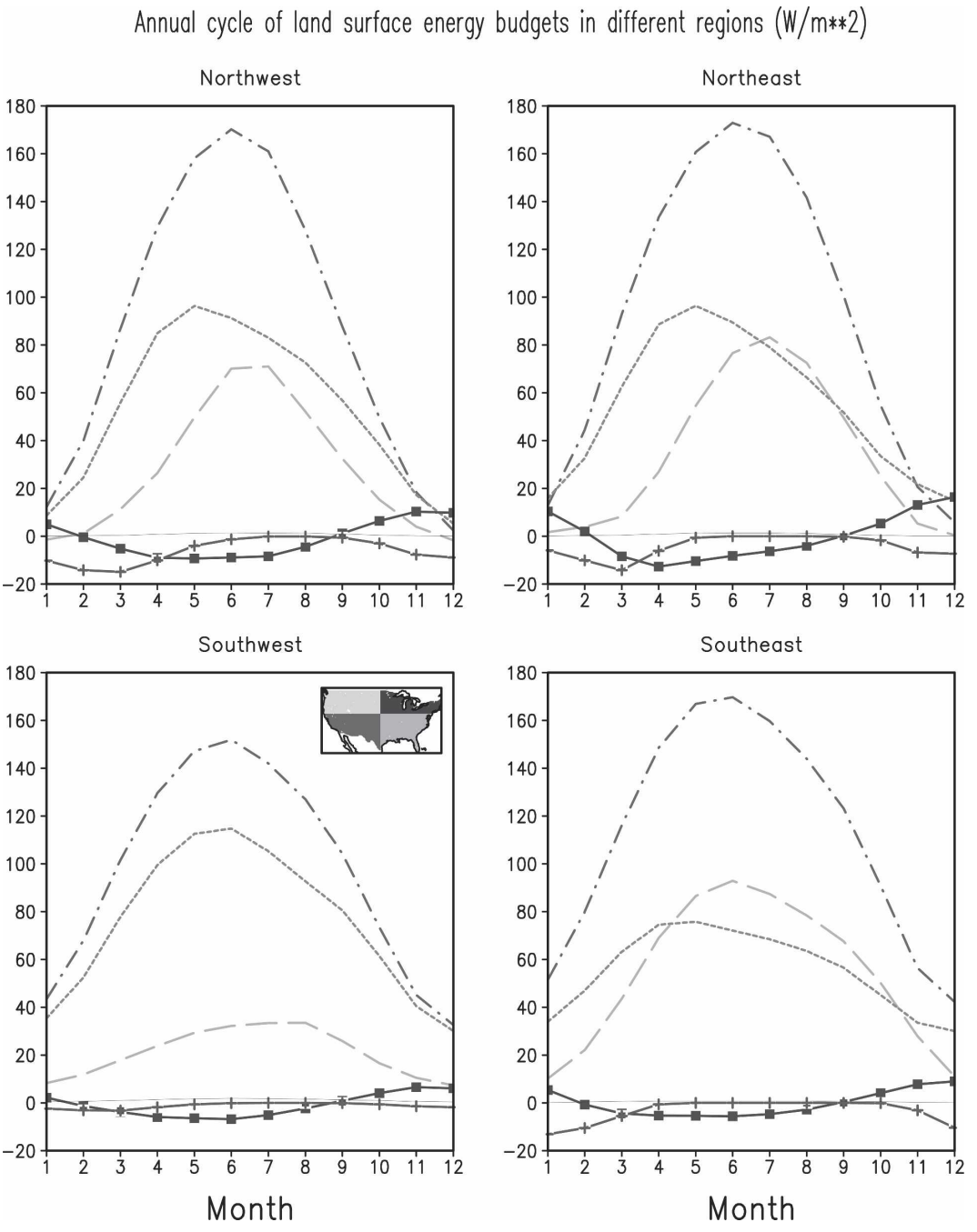

FIG. 11. The mean annual cycle of land surface energy balance components (NSWRS–NLWRS: dash-dotted line, LHTFL: dashed line, SHTFL: dotted line, GFLUX: closed square, SNOHF: plus sign) and the energy budget residual (solid line) for 1959–98 over the four U.S. subregions: northwest, northeast, southwest, and southeast (denoted by inset in lower-left panel).

uniform weighting (1/24) to distribute the daily precipitation evenly to hourly resolution. With such uniformly disaggregated precipitation, we reran the Noah LSM for 3 yr in this fashion (hereafter test run, otherwise all of the remaining forcing fields are the same as control run). In this subsection, we quantify the impacts of the two methods used to disaggregate precipitation.

Figure 13 shows the differences of evaporation and runoff between the test run and the control run for a 3-yr (1991–93) period, averaged over the four U.S.

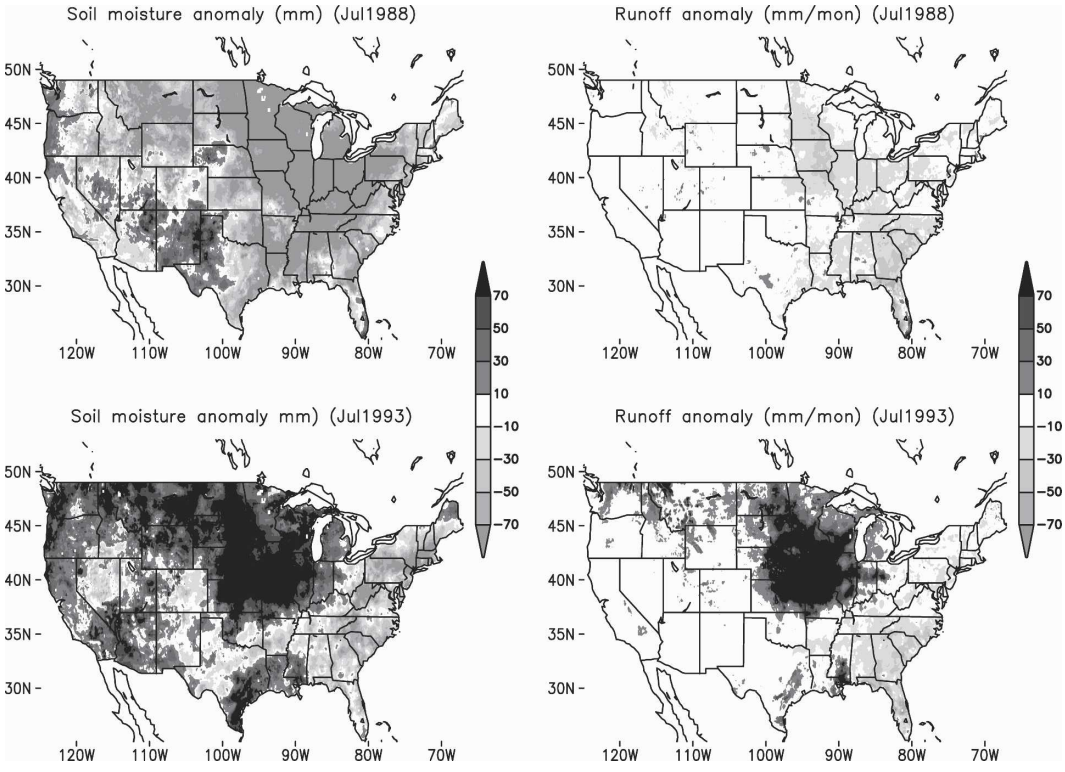

FIG. 12. Simulated extreme land surface hydrologic events: (left) soil moisture anomalies (mm) and (right) runoff anomalies (mm month^{-1}) for the 1988 drought and 1993 flood events in July.

quadrants. As expected, in general, the evaporation from the test run is slightly larger than that of the control run (except in winter), owing to much more frequent canopy moisture and higher top-layer soil moisture. However, the runoff is just the opposite, because the increased evaporation leaves less precipitation for runoff. A robust feature of the land surface skin temperature differences and soil temperature differences in all four model layers (not shown) indicates that the soil temperature in the test run is generally colder than the control run because of the increased evaporation in the test run, with differences averaged over the four U.S. quadrants ranging from 0.1° to 0.5°C for the surface layer. The magnitudes of the soil temperature differences below the surface layer are reduced with depth, and typical differences are less than 0.2°C. The impact of the different precipitation forcing on the soil moisture is relatively complicated (E and R show compensation), and the sign of the soil moisture differences between the two runs are regionally and seasonally dependent (not shown). In three of the four quadrants the soil gets wetter in the test run. The magnitudes of the soil moisture differences averaged over the four U.S. quadrants between the two runs decrease with depth. In general, the magnitudes of the soil moisture differences are around 1%–4% of the total values for the surface layer, and below the surface layer the differences are less than 1% of the total values. The above differences can be one order of magnitude larger locally. The results here show that even using the same daily precipitation but with a different hourly distribution can cause measurable differences among the land surface variables. Therefore, for land data assimilation, using more realistic and accurate hourly forcing is desirable.

4. Summary and discussions

An accurate and homogeneous land surface retrospective forcing dataset is crucial for a land surface model to realistically simulate the land surface anomalies with respect to a self-consistent long-term climatology. Thus, a retrospective 50+ year, hourly U.S. LDAS surface forcing dataset on a 1/8° grid was derived from the NCEP–NCAR Global Reanalysis. A land surface hydrological "reanalysis" over the conterminous United States has thus been completed and yielded an order of 24 variables, including all the surface energy components (at 3-hourly resolution) and water components (at daily resolution) on the 1/8° NLDAS grid for

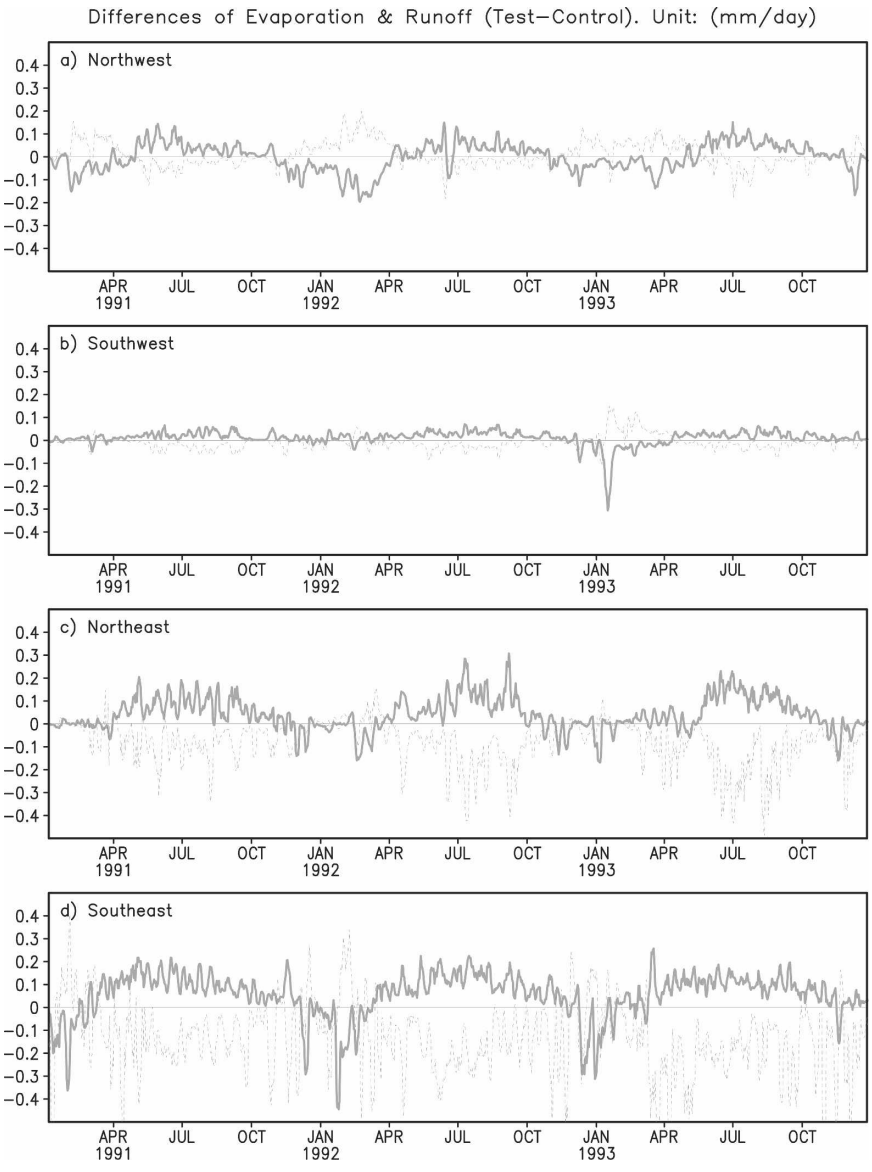

FIG. 13. Time series of the difference of 5-day running mean evaporation (thick solid) and runoff (thin dashed) of the test run (forced with uniform precipitation) minus the control run (hourly disaggregated precipitation) over the four U.S. subregions: (a) northwest, (b) southwest, (c) northeast, and (d) southeast.

1948–98. Given the ongoing real-time update at NCEP of the NCEP–NCAR Global Reanalysis, it will be straightforward in follow-on work to add the real-time update component to the land reanalysis configuration presented here.

This work is essential for improving the future NCEP real-time drought monitoring system and allowing users to quantify the severity of a drought not only in detailed spatial distribution, but also in the vertical profile. The outputs provide improved soil moisture and more extensive land surface variable dataset, such as soil temperature, snowpack, surface fluxes, etc. The retroactive run also provides superior LSM model-consistent initial conditions for numerical predictions. The early results from data validation against the soil moisture observations over Illinois show that the Noah LSM can reasonably well reproduce the observed seasonal cycle and interannual variability of the soil moisture. The simulated land surface hydrological cycle and extreme hydrologic events also look realistic. Many interesting data validation, data analysis, and model comparisons are underway. The high spatial–temporal resolution

dataset is valuable in its own right and may also be used for other studies, such as the temporal–spatial evolution of land surface energy and water budgets in different terrain and geographical locations. These studies are important for understanding land memory processes, evaluating, developing, and improving land surface models, and eventually improving our understanding of weather and climate change.

By late 2003 the North America Regional Reanalysis (NARR; 1979–present, which uses the same Noah land surface model and precipitation forcing as the Retrospective U.S. LDAS Project, albeit at lower resolution) was completed (Mesinger et al. 2004; Mitchell et al. 2004b). The availability of this new dataset opens unique possibilities for a number of validation, intercomparison, and data studies, such as with the Noah LSM 50+ year NLDAS reported in this paper and the VIC LSM 1950–2000 NLDAS (Maurer et al. 2002), which used different procedures for deriving the surface forcing from observed precipitation and air temperature, including empirically derived downward solar and longwave radiation and vapor pressure.

Although we believe the Noah LSM is an improvement over the H96 single-layer bucket model used at CPC, we do not want to overstate the gains and also need to mention some caveats. Among the advantages of the Noah land model we cite the comprehensive nature of the approach, yielding more output variables and being physically more faithful to nature, and thus most likely the route for more improvements in the future. The measurable improvement (of Noah LSM versus H96) through verification over 1984–98 against observed soil moisture over Illinois is evident in an improved annual cycle (much better phasing) and a somewhat higher anomaly correlation for the simulated anomalies, especially in central and southern Illinois. But, we are nowhere near perfection. A peculiar aspect of running a comprehensive model is the detailed nature of the output, most of which cannot be validated. To the extent to which the Noah LSM output can be validated, for example, the vertical structure of soil moisture anomalies in Illinois, we illustrated problems not seen before when only vertical integrals were compared to observations. Specifically, the simulated soil moisture anomalies of the Noah LSM showed notably less vertical gradients than the observations. The most likely cause is the uniform profile of root density applied in the Noah LSM, an attribute that needs revision in future upgrades.

A problem with the Noah LSM, versus the simpler H96, is the need for seven forcing datasets (versus the two needed for H96). These datasets, generally speaking, are not well validated in their own right. Keeping these datasets up to date in a homogeneous fashion (avoiding artificial trends) is a formidable challenge. The exact compromise between the simplicity of the models and forcing datasets and the gains to be made with the more comprehensive approaches is yet to be determined.

Acknowledgments. The authors thank Jin Huang who started this work. We also thank Sarah Lu and Wei Shi for internal review and the anonymous reviewers for their excellent comments. This project was supported by the GCIP Grant GC00-095 and GAPP Grant GC04-039.

APPENDIX A

Procedures for Elevation Adjustment

1) First, 2-m air temperature is adjusted on each NLDAS grid based on

$$T_{\mathrm{NLDAS}} = T_{\mathrm{REAN}} + \gamma \Delta Z, \tag{A1}$$

where T_{NLDAS} is the resulting NLDAS 2-m air temperature and T_{REAN} is the input NNGR 2-m air temperature interpolated to the NLDAS grid, the lapse rate $\gamma = -0.0065^{\circ}\ \mathrm{m}^{-1}$, and $\Delta Z = Z_{\mathrm{NLDAS}} - Z_{\mathrm{REAN}}$, where Z_{NLDAS} is the NLDAS topography and Z_{REAN} is the NNGR topography, interpolated to the NLDAS grid.

2) Next, the adjusted 2-m air temperature above is used to adjust the surface pressure. Based on the hydrostatic assumption and ideal gas law, that is,

$$\frac{\partial p}{\partial Z} = -\rho g \quad \text{and} \quad p = \rho R T, \tag{A2}$$

where p is pressure, Z is height, ρ is density, g is gravity, and R is the gas constant, one can derive

$$\partial Z = -\frac{RT}{g}\frac{\partial p}{p}, \tag{A3}$$

which when integrated yields

$$\Delta Z = \frac{RT_{\mathrm{MEAN}}}{g} \ln\left(\frac{p_{\mathrm{REAN}}}{p_{\mathrm{NLDAS}}}\right). \tag{A4}$$

To obtain (A4), we have applied the mean value theorem to (A3) to get

$$\int T d(\ln P) = T_{\mathrm{MEAN}} \int d(\ln P) = T_{\mathrm{mean}}\left[\ln\left(\frac{P_{\mathrm{REAN}}}{P_{\mathrm{NLDAS}}}\right)\right], \tag{A5}$$

and then assumed

$$\frac{T_{\mathrm{NLDAS}} + T_{\mathrm{REAN}}}{2} = \overline{T} = T_{\mathrm{MEAN}}; \tag{A6}$$

therefore,

$$p_{\mathrm{NLDAS}} = \frac{p_{\mathrm{REAN}}}{\exp\left(\dfrac{g\Delta Z}{RT_{\mathrm{MEAN}}}\right)}. \tag{A7}$$

3) Third, to reflect the adjusted surface temperature, the downward longwave radiation (LW) is adjusted based on the Stefan–Boltzmann law. Starting from

$$\mathrm{LW} = \varepsilon\sigma T^4, \tag{A8}$$

where ε is emissivity and σ is the Stefan–Boltzmann constant, one obtains

$$\frac{\mathrm{LW}_{\mathrm{NLDAS}}}{\mathrm{LW}_{\mathrm{REAN}}} = \frac{\varepsilon\sigma}{\varepsilon\sigma}\left(\frac{T_{\mathrm{NLDAS}}}{T_{\mathrm{REAN}}}\right)^4, \tag{A9}$$

and thus

$$\mathrm{LW}_{\mathrm{NLDAS}} = \left(\frac{T_{\mathrm{NLDAS}}}{T_{\mathrm{REAN}}}\right)^4 \mathrm{LW}_{\mathrm{REAN}}. \tag{A10}$$

4) Finally, the specific humidity (q) is adjusted based on the following assumptions: 1) maintain the 2-m relative humidity of the NNGR and, 2) given the new 2-m air temperature, find the new q required for 1 to still hold. Combining the equation of state of water vapor and dry air with the definition of specific humidity, one has the following relationships:

$$\mathrm{qsat}_{\mathrm{NLDAS}} = \frac{0.622\mathrm{esat}_{\mathrm{NLDAS}}}{p_{\mathrm{NLDAS}} - (0.378\mathrm{esat}_{\mathrm{NLDAS}})}, \tag{A11}$$

$$\mathrm{qsat}_{\mathrm{REAN}} = \frac{0.622\mathrm{esat}_{\mathrm{REAN}}}{p_{\mathrm{REAN}} - (0.378\mathrm{esat}_{\mathrm{REAN}})}, \tag{A12}$$

where qsat is the saturated specific humidity and esat is the saturated vapor pressure. According to Wexler's saturated water vapor pressure equation,

$$\mathrm{esat}_{\mathrm{NLDAS}} = 6.122\exp\left[\frac{17.67(T_{\mathrm{NLDAS}} - 273.15)}{(T_{\mathrm{NLDAS}} - 273.15) + 243.5}\right], \tag{A13}$$

$$\mathrm{esat}_{\mathrm{REAN}} = 6.122\exp\left[\frac{17.67(T_{\mathrm{REAN}} - 273.15)}{(T_{\mathrm{REAN}} - 273.15) + 243.5}\right], \tag{A14}$$

$$\mathrm{RH}_{\mathrm{REAN}} = \frac{q_{\mathrm{REAN}}}{\mathrm{qsat}_{\mathrm{REAN}}}100; \tag{A15}$$

therefore, the adjusted 2-m specific humidity can be written as

$$q_{\mathrm{NLDAS}} = \frac{\mathrm{RH}_{\mathrm{REAN}}\mathrm{qsat}_{\mathrm{NLDAS}}}{100}. \tag{A16}$$

APPENDIX B

Data Format and Categories

In some detail, the full dataset is organized as follows:

1) The "initial conditions," that is, the restart files (labeled 23Z) from the Retrospective U.S. LDAS Project are in binary format and stored once per day. They include the following state variables:
   - SMC: total volumetric soil moisture (liquid and frozen) in each soil layer,
   - SH2O: liquid volumetric soil moisture in each soil layer,
   - STC: temperature in each soil layer,
   - T1: land surface skin temperature,
   - CMC: canopy water content,
   - SNOWH: snow depth,
   - SNEQV: water equivalent snow depth.
2) The outputs of the Retrospective U.S. LDAS Project are in GRIB format and can be divided into the following two groups:
   (a) The first group (file name: *.NOAH_h.grb) includes eight "flux" variables (energy balance components): net surface shortwave and longwave radiations, latent heat flux, sensible heat flux, ground heat flux, snow phase change heat flux, and downward surface shortwave and longwave radiations. The flux terms are averaged over 3 h and stored eight times (end at 0200, 0500, 0800, 1100, 1400, 1700, 2000, and 2300 UTC) per day. More detailed information for the eight flux variables can be found in Table 1. The instantaneous land surface skin temperature is also saved in 3-h intervals with this group of data. The data can be used to study the temporal–spatial features of the land surface energy flux variables and land surface skin temperature from diurnal to seasonal and interannual time scales.
   (b) The second group (file names: *.NOAH_d.grb and *.NOAH_dd.grb) consists of 15 variables of water balance components and surface and subsurface state variables as follows: soil temperature, soil moisture (liquid plus frozen) and liquid soil moisture (i.e., unfrozen) for 0–10, 10–40, 40–100, and 100–200 cm, snowfall, rainfall, total

evaporation, surface runoff, subsurface runoff, snowmelt, snowpack water equivalent, plant canopy surface water storage, snow evaporation, potential evaporation, and snow depth and snow cover. The Noah LSM uses surface air temperature (T_a) to determine whether precipitation is rainfall (when $T_a > 273.15$ K, unfrozen precipitation) or snowfall (when $T_a \leq 273.15$ K, frozen precipitation). Here rainfall and snowfall will be mutually exclusive at any grid point for the 15-min time step. The variables are either daily accumulations or daily means, except for three state variables: soil temperature, soil moisture, and liquid soil moisture in four model layers, which are the instantaneous values at 2300 UTC. These 15 variables are stored once per day in the file *.NOAH_d.grb. For convenience, daily averaged soil temperature, soil moisture, and liquid soil moisture in four model layers are stored in the companion file *.NOAH_dd.grb.

REFERENCES

Berbery, E., K. Mitchell, S. Benjamin, T. Smirnova, H. Ritchie, R. Hogue, and E. Radeva, 1999: Assessment of land-surface energy budgets from regional and global models. *J. Geophys. Res.,* **104** (D16), 19 329–19 348.

Cosgrove, B. A., and Coauthors, 2003a: Real-time and retrospective forcing in the North American Land Data Assimilation System (NLDAS) project. *J. Geophys. Res.,* **108,** 8842, doi:10.1029/2002JD003118.

——, and Coauthors, 2003b: Land surface model spin-up behavior in the North American Land Data Assimilation System (NLDAS). *J. Geophys. Res.,* **108,** 8845, doi:10.1029/2002JD003316.

Daly, C., R. Neilson, and D. Phillips, 1994: A statistical-topographic model for mapping climatological precipitation over mountainous terrain. *J. Appl. Meteor.,* **33,** 140–158.

Delworth, T., and S. Manabe, 1988: The influence of potential evaporation on the variabilities of simulated soil wetness and climate. *J. Climate,* **1,** 523–547.

——, and ——, 1993: Climate variability and land surface processes. *Adv. Water Resour.,* **16,** 3–20.

Dirmeyer, P., 2000: Using a global soil wetness data set to improve seasonal climate simulation. *J. Climate,* **13,** 2900–2922.

Ek, M. B., K. E. Mitchell, Y. Lin, E. Rogers, P. Grunmann, V. Koren, G. Gayno, and J. D. Tarplay, 2003: Implementation of Noah land surface model advances in the National Centers for Environmental Prediction operational mesoscale Eta model. *J. Geophys. Res.,* **108,** 8851, doi:10.1029/2002JD003296.

Fennessy, M., and Shukla, J. 1999: Impact of initial soil wetness on seasonal atmospheric predictions. *J. Climate,* **12,** 3167–3180.

Gutman, G., and A. Ignatov, 1998: The derivation of the green vegetation fraction from NOAA/AVHRR data for use in numerical weather prediction models. *Int. J. Remote Sens.,* **19,** 1533–1543.

Hansen, M. C., R. S. DeFries, J. R. G. Townshend, and R. Sohlberg, 2000: Global land cover classification at 1 km spatial resolution using a classification tree approach. *Int. J. Remote Sens.,* **21,** 1331–1364.

Higgins, R. W., W. Shi, E. Yarosh, and R. Joyce, 2000: *Improved United States Precipitation Quality Control System and Analysis*. NCEP/Climate Prediction Center Atlas No. 7, 40 pp.

——, ——, ——, and J. Shaake, 2004: New orographic adjustments improve precipitation analysis for GAPP. *GEWEX News,* Vol. 14, May Issue, 8–9.

Hollinger, S. E., and S. A. Isard, 1994: A soil moisture climatology of Illinois. *J. Climate,* **7,** 822–833.

Huang, J., and H. M. Van den Dool, 1993: Monthly precipitation–temperature relation and temperature prediction over the U.S. *J. Climate,* **6,** 1111–1132.

——, ——, and K. P. Georgakakos, 1996: Analysis of model-calculated soil moisture over the United States (1931–1993) and applications to long-range temperature forecasts. *J. Climate,* **9,** 1350–1362.

Kalnay, E., and Coauthors, 1996: The NCEP/NCAR 40-Year Reanalysis Project. *Bull. Amer. Meteor. Soc.,* **77,** 437–471.

Kanamitsu, M., W. Ebisuzaki, J. Woolen, S.-Y. Yang, J. Hnilo, M. Fiorino, and G. Potter, 2002: NCEP-DOE AMIP-II Reanalysis (R-2). *Bull. Amer. Meteor. Soc.,* **83,** 1631–1643.

——, C. Lu, J. Schemm, W. Ebisuzaki, 2003: The predictability of soil moisture and near-surface temperature in hindcasts of the NCEP seasonal forecast model. *J. Climate,* **16,** 510–521.

Kistler, R., and Coauthors, 2001: The NCEP–NCAR 50-Year Reanalysis: Monthly means CD-ROM and documentation. *Bull. Amer. Meteor. Soc.,* **82,** 247–268.

Koster, R. D., and M. J. Suarez, 2001: Soil moisture memory in climate models. *J. Hydrometeor.,* **2,** 558–570.

——, ——, and M. Heiser, 2000: Variance and predictability of precipitation at seasonal-to-interannual timescales. *J. Hydrometeor.,* **1,** 26–46.

——, ——, R. W. Higgins, and H. M. Van den Dool, 2003: Observational evidence that soil moisture variations affect precipitation. *Geophys. Res. Lett.,* **30,** 1241, doi:10.1029/2002GL016571.

Liang, X., D. P. Lettenmaier, E. Wood, and S. J. Burges, 1994: A simple hydrologically based model of land surface water and energy fluxes for general circulation models. *J. Geophys. Res.,* **99** (D7), 14 415–14 428.

Mahrt, L., and H. Pan, 1984: A two-layer model of soil hydrology. *Bound.-Layer Meteor.,* **29,** 1–20.

Manabe, S., 1969: Climate and the ocean circulation. *Mon. Wea. Rev.,* **97,** 739–774.

Maurer, E. P., G. M. O'Donnell, D. P. Lettenmaier, and J. O. Roads, 2001: Evaluation of the land surface water budget in NCEP-NCAR and NCEP-DOE reanalysis using an off-line hydrologic model. *J. Geophys. Res.,* **106** (D16), 17 841–17 862.

——, A. W. Wood, J. C. Adam, D. P. Lettenmaier, and B. Nijssen, 2002: A long-term hydrologically based dataset of land surface fluxes and states for the conterminous United States. *J. Climate,* **15,** 3237–3251.

Mesinger, F., and Coauthors, 2004: NCEP North America Regional Reanalysis. Preprints, *15th Symp. on Global Change and Climate Variations,* Seattle, WA, Amer. Meteor. Soc., CD-ROM, P1.1.

Miller, D. A., and R. A. White, 1998: A conterminous United States multi-layer soil characteristics data set for regional climate and hydrology modeling. *Earth Interactions,* **2**. [Available online at http://EarthInteractions.org.]

Mintz, Y., and G. K. Walker, 1993: Global fields of soil moisture and land surface evapotranspiration derived from observed precipitation and surface air temperature. *J. Appl. Meteor.,* **32,** 1305–1334.

Mitchell, K., and Coauthors, 2004a: The multi-institution North American Land Data Assimilation System (NLDAS): Utilizing multiple GCIP products and partners in a continental distributed hydrological modeling system. *J. Geophys. Res.,* **109,** D07S90, doi:10.1029/2003JD003823.

——, and Coauthors, 2004b: NECP completes 25-year North American Reanalysis: Precipitation assimilation and land surface are two hallmarks. *GEWEX News,* Vol. 14, May Issue, 9–12.

Namias, J., 1952: The annual course of month-to-month persistence in climatic anomalies. *Bull. Amer. Meteor. Soc.,* **33,** 279–285.

Reed, C. D., 1925: Monthly forecasts by correlation. *Mon. Wea. Rev.,* **53,** 249–251.

Roads, J., and Coauthors, 2003: GCIP Water and Energy Budget Synthesis (WEBS). *J. Geophys. Res.,* **108,** 8609, doi:10.1029/2002JD002583.

Robock, A., K. Y. Vinnikov, G. Srinivasan, J. K. Entin, S. E. Hollinger, N. A. Speranskaya, S. Liu, and A. Namkhai, 2000: The Global Soil Moisture Data Bank. *Bull. Amer. Meteor. Soc.,* **81,** 1281–1299.

Rodell, M., and Coauthors, 2003: The Global Land Data Assimilation System. *Bull. Amer. Meteor. Soc.,* **85,** 381–394.

Schaake, J. C., and Coauthors, 2004: An intercomparison of soil moisture fields in the North American Land Data Assimilation System (NLDAS). *J. Geophys. Res.,* **109,** D01S90, doi:10.1029/2002JD003309.

Schaefer, G. L., and R. F. Paetzold, 2001: SNOTEL (SNOwpack TELemetry) and SCAN (Soil Climate Analysis Network). *Proc. Int. Workshop on Automated Weather Stations for Applications in Agriculture and Water Resource Management,* High Plains Climate Center, University of Nebraska—Lincoln and WMO, World Meteorological Organization AGM-3 WMO/TD 1074.

Torrence, C., and P. J. Webster, 1998: The annual cycle of persistence in the El Nino/Southern Oscillation. *Quart. J. Roy. Meteor. Soc.,* **124,** 1985–2004.

Van den Dool, H. M., J. Huang, and Y. Fan, 2003: Performance and analysis of the constructed analogue method applied to U.S. soil moisture over 1981–2001. *J. Geophys. Res.,* **108,** 8617, doi:10.1029/2002JD003114.

van den Hurk, B., 2002: European LDAS established. *GEWEX News,* Vol. 12, May Issue, 9.

Verdin, K. L., and S. K. Greenlee, 1996: Development of continental scale digital elevation models and extraction of hydrographic features. *Proc. Third Int. Conf./Workshop on Integrating GIS and Environmental Modeling,* Santa Fe, NM, National Center for Geographic Information and Analysis, National Center for Geographic Information Analysis, University of California, Santa Barbara, CD-ROM. [Available from NCGIA, 3510 Phelps Hall, University of California, Santa Barbara, CA 93106.]

Wahr, J., S. Swenson, V. Zlotnicki, and I. Velincogna, 2004: Time-variable gravity from GRACE: First results. *Geophys. Res. Lett.,* **31,** L11501, doi:10.1029/2004GL019779.

Yeh, T.-C., 1989: Sensitivity of climate model to hydrology. *Understanding Climate Change,* A. Berger, R. E. Dickinson, and J. W. Kidson, Eds., Amer. Geophys. Union, 100–108.